AD 422359

nato

NOLTR 63-77

422359

A SEMI-EMPIRICAL DERIVATION OF FRICTION, HEAT-TRANSFER, AND MASS-TRANSFER COEFFICIENTS FOR THE CONSTANT PROPERTY TURBULENT BOUNDARY LAYER ON A FLAT PLATE

NOL

3 JULY 1963

UNITED STATES NAVAL ORDNANCE LABORATORY, WHITE OAK, MARYLAND

NOLTR 63-77

A SEMI-EMPIRICAL DERIVATION OF FRICTION, HEAT-TRANSFER, AND MASS-TRANSFER COEFFICIENTS FOR THE CONSTANT PROPERTY TURBULENT BOUNDARY LAYER ON A FLAT PLATE

by

Neal Tetervin

ABSTRACT: The friction coefficient and velocity profile are calculated from the relation between the shear, the sum of the molecular and eddy viscosity, and the velocity gradient. The non-dimensional shear distribution is assumed to be fixed. The eddy viscosity across the boundary layer is obtained by joining a distribution for the wall region to one for the outer region. By use of the shear and eddy viscosity distributions the velocity profile is calculated from the wall to the outer edge of the boundary layer for all Reynolds numbers without using the concept of laminar sublayer, transition region, logarithmic region, etc.

The heat and mass transfer coefficients and the temperature and concentration profiles are calculated by a similar method.

PUBLISHED OCTOBER 1963

U. S. NAVAL ORDNANCE LABORATORY
WHITE OAK, MARYLAND

NOLTR 63-77

3 July 1963

A Semi-Empirical Derivation of Friction, Heat Transfer, and Mass-Transfer Coefficients for the Constant Property Turbulent Boundary Layer on a Flat Plate

This report presents the results of a theoretical investigation of the constant property turbulent boundary layer on a flat plate. A new method of analysis that obtains many of the results previously obtained by a number of different approaches is introduced. The new method also yields some results not previously available from theoretical analyses.

This work was sponsored by the Re-Entry Body Section of the Special Projects Office, Bureau of Naval Weapons, under the Applied Research Program in Aeroballistics, Task No. NOL 364.

R. E. ODENING
Captain, USN
Commander

K. R. EMKENHUS
By direction

CONTENTS

ILLUSTRATIONS

TABLES

SYMBOLS

C_f	local friction coefficient, $\frac{\tau}{\frac{\rho u_e^2}{2}}$
C_F	average friction coefficient, $\frac{1}{x}\int_0^x C_f dx$
C_l	mass concentration of species l
C_m	mass-transfer coefficient $\frac{-m_{lw}}{\rho u_e (C_{le}-C_{lw})}$
C_p	specific heat at constant pressure
$\mathscr{D}$	binary diffusion coefficient
D^T	thermal diffusion coefficient
E	internal energy per unit mass
$f_o, f_1, \ldots f_{11}$	functions
k	conductivity
k_o, k_1	constants
K	von Karman's constant
m_l	mass transfer of species l per unit time per unit area
n_o, n_1	constants
Pr	Prandtl number, $\frac{C_p \mu}{k}$
q	heat transfer per unit time per unit area
r	radius of pipe
Re_f	friction Reynolds number, $\sqrt{C_f/2}\, Re_\delta$ or $\frac{u_e \delta}{\nu}$
Re_δ	boundary-layer Reynolds number, $\frac{u_e \delta}{\nu}$
Re_θ	boundary-layer momentum thickness Reynolds number, $\frac{u_e \theta}{\nu}$
Re_x	Reynolds number based on distance along plate, $\frac{u_e x}{\nu}$
S_c	Schmidt number, $\frac{\mu}{\rho \mathscr{D}}$
S_t	local Stanton number, $\frac{-q_w}{\rho u_e c_p (T_e - T_w)}$
S_T	average Stanton number, $\frac{1}{x}\int_0^x S_t dx$

T	temperature
t	temperature ratio, $\frac{T-T_w}{T_e-T_w}$
t_+	$\frac{T-T_w}{t_*}$
t_*	$S_t (T_e-T_w)/\sqrt{\frac{c_f}{2}}$
u	velocity component in x direction
u_+	ratio of local velocity, u, to friction velocity, u_*
u_*	friction velocity, $\sqrt{\frac{\tau_w}{\rho}}$
v	velocity component in y direction
x	distance in direction parallel to surface
y	distance in direction normal to surface
y_+	kinematic viscosity wall distance Reynolds number, $\frac{u_* y}{\nu}$
ϵ	eddy transfer quantity
δ	velocity boundary layer thickness
δ_c	concentration boundary layer thickness
δ_T	temperature boundary layer thickness
δ^*	boundary-layer displacement thickness, $\int_0^1 (1-\phi)\,d\eta$
η	non-dimensional distance from surface, $\frac{y}{\delta}$
η_T	non-dimensional distance from surface, $\frac{y}{\delta_T}$
θ	boundary-layer momentum thickness, $\int_0^1 \phi(1-\phi)\,d\eta$.
μ	viscosity
ν	kinematic viscosity
ξ	non-dimensional concentration ratio, $\frac{c_1-c_{1w}}{c_{1e}-c_{1w}}$
ρ	density
τ	shear stress
φ	non-dimensional velocity ratio, $\frac{u}{u_e}$

All velocities, temperatures, and concentrations are average values.

Subscripts

d	diffusivity
e	at outer edge of boundary layer
h	thermal diffusivity
m	kinematic viscosity
1	limit of wall region for eddy kinematic viscosity
2	limit of wall region for eddy thermal diffusivity
w	at wall

SUMMARY

A new method for the calculation of mean flow quantities in a constant property turbulent boundary layer on a flat plate is developed. In this method the friction coefficient and velocity profile are calculated from the relation between the shear, the sum of the molecular and eddy viscosity, and the velocity gradient. The shear distribution, experimentally obtained by previous investigators, is assumed to be fixed. The eddy viscosity is obtained by joining a distribution for the wall region to one for the outer region of the boundary layer. Both distributions were calculated by previous investigators from measured flow quantities. By use of the shear and eddy viscosity distributions the friction coefficient is calculated and agrees well with accepted values over the entire range of Reynolds number. For large Reynolds numbers the logarithmic friction formula is obtained.

The velocity profile is calculated by the same method as the friction coefficient. The entire profile, from the wall to the outer edge, is calculated without using the concept of laminar sublayer, transition region, logarithmic region,,etc. The calculated velocity profile changes gradually from the laminar type at small Reynolds numbers to the turbulent type at larger Reynolds numbers. For sufficiently large Reynolds numbers the logarithmic formula is obtained for one part of the velocity profile and the velocity defect formula for another part.

The heat-transfer coefficient and non-dimensional temperature profile for small temperature differences are calculated by the same method as the friction coefficient and velocity profile. In these calculations the non-dimensional heat-transfer distribution,which must be known, is assumed to be the same as the non-dimensional shear distribution. In addition to the Prandtl number, the ratio of the eddy thermal diffusivity to the eddy kinematic viscosity also appears. This ratio is calculated from experimental data obtained by previous investigators. The calculated ratio of local Stanton number to half the local friction coefficient is found to vary from about 1.22 at a Reynolds number of about 3.5×10^4, based on the distance to the leading edge, to about 1.09 at a Reynolds number of 2.2×10^9. The calculated non-dimensional temperature profiles differ slightly from the velocity profiles.

Turbulent flow over a surface on which condensation or evaporation is occurring is treated by assuming that the rate of condensation or evaporation is small, that the Schmidt number is equal to the Prandtl number, and that the eddy diffusivity is equal to the eddy thermal diffusivity. The mass-transfer coefficient is then equal to the heat-transfer coefficient, and the non-dimensional concentration profile is the same as the non-dimensional temperature profile.

INTRODUCTION

The problem of calculating the friction coefficient and velocity distribution for a constant property turbulent boundary layer is an old one. In a rigorous sense the problem is unsolved and will remain so until shear turbulence is understood better. At present the friction coefficient is usually calculated from a formula designed to fit either experimental data or the logarithmic formula (refs. (1) and (2)). The logarithmic formula is theoretically derived but contains two constants that must be found from experiment. This formula can be derived in a number of ways, for example, by use of Prandtl's or von Karman's relations for the eddy viscosity or by Millikan's method of overlap (ref. (1)).

The analyses that lead to a logarithmic friction formula also result in the logarithmic velocity profile. This velocity distribution agrees reasonably well with experiment over a portion of the boundary layer from near the edge of the laminar sublayer to about one-fifth of the boundary layer thickness from the wall. The region very close to the wall requires a separate treatment that gives the result that in this region the velocity is directly proportional to the distance from the wall. The velocity profile must vary continuously from the linear to the logarithmic, but the variation is not obtainable from either the procedure that gives the linear profile or from that which yields the logarithmic profile. A number of investigators have treated this problem (ref. (1)). To calculate the velocity distribution thus requires that the boundary layer be divided into a number of regions. This is true even if Cole's correlation of velocity profiles (ref. (1)) is used. A complete review and detailed discussion of the present knowledge of the constant property turbulent boundary layer on a flat plate is given in reference (1).

In the present analysis the velocity profile and friction coefficient are obtained from the relation between the shear, the sum of the molecular and eddy viscosity, and the velocity gradient. The shear distribution, experimentally obtained by previous investigators, is assumed to be fixed. The eddy viscosity is obtained by joining a distribution for the wall region to one for the outer region of the boundary layer. Both distributions were calculated by previous investigators from measured flow quantities. By use of the shear and eddy viscosity distributions the friction coefficient is calculated and agrees well with accepted values over the entire range of Reynolds number. For the limiting case of zero Reynolds number, the friction coefficient becomes almost equal to the exact Blasius value for laminar flow (ref. (2)). At the other extreme, very large Reynolds number, the analytic expression for the logarithmic friction formula is obtained.

The velocity profile is calculated by the same method as the friction coefficient. Unlike the usual procedure, the entire profile from the wall to the outer edge is calculated without splitting the boundary layer in a more or less arbitrary manner into laminar sublayer, transition region, logarithmic region, etc. The calculated velocity profile changes gradually from almost the exact Blasius laminar profile in the limit of zero Reynolds number to the turbulent type at larger Reynolds numbers.

The heat-transfer coefficient and temperature profile for small temperature differences are calculated in a manner similar to that for the friction coefficient and velocity profile. That is, instead of the relation between the local shear, the total viscosity, and the velocity gradient, there is used the relation between the local heat transfer, the sum of the molecular and eddy conductivity, and the temperature gradient. The information required to calculate the eddy conductivity is obtained from the experimental data of reference (3). The non-dimensional heat-transfer distribution across the boundary layer is assumed to be the same as the non-dimensional shear distribution.

For small concentration of a foreign gas, for Schmidt number equal to Prandtl number, for eddy diffusivity equal to the eddy thermal diffusivity, and for the non-dimensional mass-transfer distribution across the boundary layer equal to the non-dimensional heat-transfer distribution, the concentration profile and mass-transfer coefficient can be obtained directly from the temperature profile and heat-transfer coefficient.

ANALYSIS

Friction Coefficient and Velocity Profile

In laminar boundary layer flow the shear stress is related to the velocity gradient by the relation

$$\tau = \mu \frac{\partial u}{\partial y} \tag{1}$$

For turbulent flow, it is assumed that an eddy kinematic viscosity ϵ_m can be found such that

$$\tau = (\mu + \rho \epsilon_m) \frac{\partial u}{\partial y} \tag{2}$$

Equation (2) can be written as

$$\frac{\tau}{\tau_w} = \frac{\mu \left(1 + \frac{\epsilon_m}{\nu}\right)}{\tau_w} \frac{u_e}{\delta} \frac{\partial \frac{u}{u_e}}{\partial \frac{y}{\delta}} .$$

or, for constant property flow, as

$$\frac{\tau}{\tau_w} = \left(1 + \frac{\epsilon_m}{\nu}\right) \frac{1}{\frac{c_f}{2} Re_\delta} \frac{\partial \phi}{\partial \eta} \tag{3}$$

From (3) it follows that

$$\frac{c_f}{2} Re_\delta \int_0^1 \frac{\frac{\tau}{\tau_w}}{1 + \frac{\epsilon_m}{\nu}} d\eta = \int_0^1 \frac{\partial \phi}{\partial \eta} d\eta = 1 \tag{4}$$

Therefore

$$\frac{1}{\frac{c_f}{2} Re_\delta} = \int_0^1 \frac{\frac{\tau}{\tau_w}}{1 + \frac{\epsilon_m}{\nu}} d\eta \tag{5}$$

To evaluate the integral in (5), $\frac{\tau}{\tau_w}$ and $\frac{\epsilon_m}{\nu}$ must be known from the wall to the outer edge of the boundary layer. The ratio $\frac{\tau}{\tau_w}$, shown in figure (1), was obtained from figure 7-13 of reference (1); figure 7-13 gives the ratio of the measured turbulence shear stress to the wall shear stress. Near $\eta = 0$, the curve of $\frac{\tau}{\tau_w}$ was drawn slightly above the curve of figure 7-13 of reference (1) in order to agree more closely with the experimental points shown in that figure and also to allow for the viscous shear and to give the slope its required value of zero at the wall. In figure 1 is also shown the ratio $\frac{\tau}{\tau_w}$ calculated by Fediaevsky's method (ref. (4)). In this method the ratio $\frac{\tau}{\tau_w}$ is expressed as a fourth degree polynomial in η and the coefficients, which depend on the value of $\frac{\tau}{\tau_w}$ and its derivatives at $\eta = 0$ and at $\eta = 1$, are evaluated by use of the boundary layer equation of motion. Although Fediaevsky's distribution of $\frac{\tau}{\tau_w}$ is not very far from the measured one, the measured one was used in the present analysis. For a flat plate, Fediaevsky's method makes $\frac{\tau}{\tau_w}$ a function of η alone; the same assumption is made in this analysis.

The ratio $\frac{\epsilon_m}{\nu}$ is obtained from reference (1). The discussion on page 526 and the data of figure 7-41 of reference (1) indicate that very near the wall

$$\frac{\epsilon_m}{\nu} = f_o\left(\frac{u_\tau y}{\nu}\right)$$

or

$$\frac{\epsilon_m}{u_* y} = f_1\left(\frac{u_* y}{\nu}\right) \tag{6}$$

Relation (6) is universal under the assumption that the portion of the velocity boundary layer very near the wall can be completely described by the quantities u, ϵ_m, ρ, μ, τ_w, and y.

Further from the wall, the discussion on page 493 and the data in figure 7-17 of reference (1) indicate that

$$\frac{\epsilon_m}{u_* \delta} = f_2(\eta) \tag{7}$$

Because this relation does not contain the viscosity, it probably applies only at large Reynolds numbers. At small Reynolds numbers, $\frac{\epsilon_m}{u_* \delta}$ is probably a function of Re_δ in addition to η.

Because (6) applies only near the wall and (7) applies only further out, (5) is written as

$$\frac{1}{\frac{c_f}{2} Re_\delta} = \int_0^{\eta_1} \frac{\frac{\tau}{\tau_w}}{1 + \frac{\epsilon_m}{\nu}} d\eta + \int_{\eta_1}^{1} \frac{\frac{\tau}{\tau_w}}{1 + \frac{\epsilon_m}{\nu}} d\eta \tag{8}$$

where η_1 is the smallest value of η for which (7) applies. For $\eta < \eta_1$, $\frac{\epsilon_m}{\nu}$ depends on y_+ instead of on η. Consequently, the first integral in (8) is written as

$$\frac{1}{Re_f} \int_0^{y_{+,1}} \frac{\frac{\tau}{\tau_w}\left(\frac{y_+}{Re_f}\right)}{1 + y_+ f_1} dy_+$$

where $$Re_f = \frac{u_* \delta}{\nu} = \sqrt{\frac{c_f}{2}}\, Re_\delta$$

and $$y_+ = \frac{u_* y}{\nu} = \eta\, Re_f \tag{9}$$

and $$y_{+,1} = \eta_1\, Re_f$$

The notation $\frac{\tau}{\tau_w}\left(\frac{y_+}{Re_\epsilon}\right)$ points out that $\frac{\tau}{\tau_w}$ is assumed to be a function of $\eta\left(\equiv \frac{y_+}{Re_\epsilon}\right)$ near the wall as well as further out.

Equation (8) then becomes

$$\frac{1}{\sqrt{\frac{c_f}{2}}} = \int_0^{y_{+1}} \frac{\frac{\tau}{\tau_w}}{1+y_+ f_1}\, dy_+ + Re_\epsilon \int_{\eta_1}^{1} \frac{\frac{\tau}{\tau_w}}{1+Re_\epsilon f_2}\, d\eta \qquad (10)$$

The function $f_2(\eta)$ was obtained directly from the faired curve in figure 7-17 of reference (1) and is shown in figure 2. The function $f_1(y_+)$ was obtained from figures 7-16 and 7-41 of reference (1) and is shown in figure 3. The points are the data points of figures 7-16 and 7-41 of reference (1). For $15 < y_+ < 52$, the curve of f_1 in figure 3 is a slightly adjusted version of the curve of figure 7-16 of reference (1). The data of reference (1) do not indicate an upper limit to the rising portion of f_1. In the present analysis, however, f_1 is postulated to have the constant value .393 for a range of $y_+ > 52$ if Re_ϵ is sufficiently large. The function f_1 is postulated to have this constant portion because if, at a sufficiently large value of Re_ϵ, f_2 is plotted against y_+ by use of (9) and the identity

$$\frac{\epsilon_m}{u_* y} = \left(\frac{\epsilon_m}{u_* \delta}\right)\frac{1}{\eta} \qquad (11)$$

the portion of f_2 for η less than about .06 in figure 2 with a slope of .393 lies on the line $\epsilon_m/u_* y = .393$ in figure 3. Therefore, $\epsilon_m/u_* y$ would be double valued for $y_+ > 52$ unless f_1 either did not extend beyond $y_+ = 52$ or were equal to f_2 beyond $y_+ = 52$. By taking $f_1 = .393$ for $y_+ > 52$, it is not necessary to limit the range of f_1 by the fixed number 52. Moreover, making f_1 extend beyond $y_+ = 52$ necessitates that $f_2 = K\eta$ in the region of the boundary layer in which f_1 and f_2 apply simultaneously. Thus, from (6) it follows that

$$\frac{\epsilon_m}{u_* \delta} = \eta f_1(y_+)$$

Therefore, where (6) and (7) are both valid it is necessary that

$$f_1(y_+) = K$$

and

$$f_2(\eta) = K\eta \quad (K \simeq .393) \tag{12}$$

At high Reynolds numbers the upper limit of f_1 is thus postulated to be the largest value of y_+ for which $f_1 = K$, that is, at about .06 Re_f.

The lower limit η_1 for f_2 is found by first calculating $\frac{\epsilon_m}{u_\tau y}$ from $f_2(\eta)$ by (11) and then, by use of (9), plotting these values of $\frac{\epsilon_m}{u_\tau y}$ together with f_1 as shown in figure 4. The extension of f_2 down to $y_+ = 0$ is merely for the purpose of calculating η_1. When f_1 and f_2 intersect at $y_+ < 52$, the value of y_+ at the intersection is $y_{+,1}$. Equation (9) then gives η_1. When there is no intersection at $y_+ < 52$, $y_{+,1}$ is 52 and η_1 is $\frac{52}{Re_f}$. The curve of f_2 for $Re_f = 2960$ in figure 4 is an example of a Reynolds number that is so large that f_1 and f_2 do not intersect for $y_+ < 52$. Therefore, 52 is used for $y_{+,1}$. The curve for $Re_f = 200$ shows the behavior at a low Reynolds number. Here, f_1 and f_2 intersect at $y_+ < 52$. When the Reynolds numbers are so low that $y_{+,1} < 52$, then $y_{+,1}$ depends on Re_f.

By use of figures 1, 2, and 3, and this method for finding $y_{+,1}$ and η_1, the value of $C_f/2$ was calculated from (10) for six values of Re_f. The values of $y_{+,1}$ and η_1 and the corresponding values of f_1 and f_2 for the three values of Re_f for which $y_{+,1}$ is less than 52 are given in Table I. In Table II are listed the values of $C_f/2$ and Re_δ. The value of $\sqrt{C_f/2}$ for $Re_f = 2960$, namely .0373, is almost the same as the value .037 given in reference (1). In figure 5 the calculated values of $C_f/2$ are compared with those obtained by use of the logarithmic velocity profile and given in Table 21.1 of reference (2). The agreement is good over the entire range of Re_f. It is noted, however, that because (7) does not contain the viscosity, it is probably valid only at large Reynolds numbers. At small Reynolds numbers the function f_2 is probably somewhat different from that shown in figure 2 with the result that $C_f/2$ is also probably different from that calculated.

The velocity profile is obtained by solving equation (3) for $\frac{\partial \Phi}{\partial \eta}$ and integrating between 0 and η. Thus,

$$\Phi = \frac{C_f}{2} Re_\delta \int_0^\eta \frac{\frac{\tau}{\tau_w}}{1 + \frac{\epsilon_m}{\nu}} d\eta \tag{13}$$

For the same reason that (5) was written as (8), (13) is written as

$$\phi = \sqrt{\frac{C_f}{2}} \int_0^{y_+} \frac{\frac{\tau}{\tau_w}}{1 + y_+ f_1} \, dy_+ \qquad (14)$$

for $y_+ \leq y_{+,1}$, and as

$$\phi = \sqrt{\frac{C_f}{2}} \int_0^{y_{+1}} \frac{\frac{\tau}{\tau_w}}{1 + y_{+,1} f_1} \, dy_+ + \frac{C_f}{2} Re_\delta \int_{\eta_1}^{\eta} \frac{\frac{\tau}{\tau_w}}{1 + Re_f f_2} \, d\eta \qquad (15)$$

for $\eta > \eta_1$. The velocity profiles, $\phi(\eta)$, are tabulated in Table III and shown in figure 6 for the six values of Re_f for which $C_f/2$ was calculated. Because there is a unique relation between Re_f and $C_f/2$, it follows that the velocity profile is uniquely related to $C_f/2$. Included in Table III and figure 6 is the profile for laminar flow. This profile was calculated by using the same $\frac{\tau}{\tau_w}$ distribution as for turbulent flow, that shown in figure 1, and by putting $\frac{\epsilon_m}{\nu}$ equal to zero in equation (5) to get

$$\frac{C_f}{2} Re_\delta = \left[\int_0^1 \frac{\tau}{\tau_w} \, d\eta \right]^{-1} = 1.826 \qquad (16)$$

This result was then used in (13) to get

$$\phi = \frac{C_f}{2} Re_\delta \int_0^{\eta} \frac{\tau}{\tau_w} \, d\eta = 1.826 \int_0^{\eta} \frac{\tau}{\tau_w} \, d\eta \qquad (17)$$

The velocity profiles in figure 6 show a gradual change from the laminar to the turbulent type as Re_f increases.

Note that both the friction coefficient and velocity profile become exactly those for laminar flow when the Reynolds number becomes zero. Thus, $\frac{\epsilon_m}{\nu}$ in (5) and (13) can be written as $\left(\frac{\epsilon_m}{u_\tau \delta}\right) \sqrt{\frac{C_f}{2}} Re_\delta$. Then, as Re_δ decreases to zero $\frac{\epsilon_m}{\nu}$ also decreases to zero because the friction Reynolds number, $\sqrt{C_f/2}\, Re_\delta$, is zero for Re_δ equal to zero. Equations (5) and (13) then become (16) and (17), respectively, the equations for laminar flow.

In figure 7 all the velocity profiles of figure 6 except the laminar one are shown in the form u_+ against y_+. The relation between u_+ and ϕ is

$$u_+ = \frac{\phi}{\sqrt{\frac{C_f}{2}}} \qquad (18)$$

and the relation between y_+ and η is given by (9). Each velocity profile has a straight line portion that lies on the single line which is fitted by the equation

$$u_+ = 2.54 \ln y_+ + 3.89$$

Each velocity profile leaves this line at a sufficiently large value of u_+. Calculations indicate that this occurs when Φ exceeds about .75.

The profile for $Re_f = 25$ lies markedly below all the others. The reason is that 25 is so small a value of Re_f that large values of η occur for small values of y_+ (see eq. (9)). Consequently, $\frac{\tau}{\tau_w}$, which is assumed to depend on η alone, is smaller over the range of integration in (15) than it is for larger values of Re_f. For example, at $y_+ = 12.2$, which is $y_{+,1}$ in this case, η is large enough for $\frac{\tau}{\tau_w}$ to equal .600, a value appreciably less than unity. As a result u_+ is small over the entire boundary layer and its maximum value is only 9.31.

In figure 7 are also shown Klebanoff's data for $Re_f = 2960$ from figure 21 of reference (5). Klebanoff's data differ slightly from the curve of the present analysis for values of y_+ between about 20 and 120. If the curve of f_1 of reference (1) had been used without refairing it, better agreement would have been obtained with Klebanoff's data.

In figure 3 are shown the computed velocity profiles in the form $\frac{u_e - u}{u_\tau}$ against η. Also shown is the curve from figure 7-4 of reference (1); this curve is a mean through experimental data. There is fair agreement between the calculated velocity profiles and this mean curve for the three largest values of Re_f but not for the three smallest values. The three smallest Reynolds numbers are probably much smaller than those for which data were used to construct the curve of figure 7-4 of reference (1). The comparisons with experiment in figures 7 and 3 indicate that a calculated profile probably differs slightly from an experimental one at the same friction Reynolds number.

From the computed velocity profiles the quantities $\frac{\theta}{\delta}$ and $\frac{\delta^*}{\delta}$ were calculated numerically from their definitions, namely,

$$\frac{\theta}{\delta} = \int_0^1 \Phi(1-\Phi)\,d\eta$$

and

$$\frac{\delta^*}{\delta} = \int_0^1 (1-\Phi)\,d\eta$$

The ratio $\frac{\delta^*}{\theta}$ was calculated from $\frac{\delta^*}{\theta} = \left(\frac{\delta^*}{\delta}\right)\left(\frac{\delta}{\theta}\right)$

These quantities are given in Table IV. By use of $\frac{\theta}{\delta}$, the value of Re_θ, a more convenient quantity than Re_δ or Re_f, was calculated for each value of Re_f for which $C_f/2$ was computed. These values of Re_θ are given in Table IV and the dependence of $C_f/2$ on Re_θ is shown in figure 9.

When $C_f/2$ is known as a function of Re_θ, the dependence of $C_f/2$ and of C_F on Re_x can be calculated. The procedure is to use the boundary layer momentum equation in the form

$$\frac{dRe_\theta}{dRe_x} = \frac{C_f}{2} \tag{19}$$

which, upon integration, gives

$$Re_x = \int_0^{Re_\theta} \frac{2}{C_f}\, dRe_\theta \qquad (\theta = 0 \text{ at } x = 0) \tag{20}$$

The relation

$$C_F = 2\frac{Re_\theta}{Re_x} \tag{21}$$

is also used.

To calculate Re_x from (20), $C_f/2$ must be known as a function of Re_θ for small values of Re_θ. In the present analysis the turbulent boundary layer gradually becomes laminar as Re_θ approaches zero so that it is unnecessary to assume either a turbulent boundary layer at the leading edge or a transition position. In order to use (20), $C_f/2$ was extrapolated from its value at Re_θ equal to 27.7 down to zero by fitting the equation

$$\frac{C_f}{2} = \frac{k_o}{Re_\theta^{n_o}}$$

to the values of $C_f/2$ at $Re_\theta = 27.7$ and 191 (see Tables II and IV). It was found that $k_o = .0789$ and $n_o = .5785$. For $Re_\theta = 100$ equation (20) then gives $Re_x = 11{,}530$ and equation (21) gives $C_F = .01735$. Although k_o and n_o should approach their laminar values, namely, .2205 and 1, instead of remaining fixed as Re_θ becomes zero, it can be shown that at $Re_\theta = 100$ the error in Re_x caused by keeping k_o and n_o fixed is no larger than 2 percent. The percentage error in Re_x and C_F decreases as Re_θ increases. For values of Re_θ larger than 100, equation (20) was integrated numerically by use of figure 9. In figure 10 is shown the calculated dependence of C_F on Re_x; also shown is the dependence of C_F on Re_x predicted by the Prandtl-Schlichting and Schultz-Grunow formulas (ref. (2)). The agreement is good.

In figure 11 is shown the connection between Re_θ and Re_x calculated by use of (20). Figure 11 is given because it enables quantities known as a function of Re_θ to be easily obtained as a function of Re_x and vice versa. Thus, from this figure and figure 9 the dependence of $C_f/2$ on Re_x can be found.

Heat-Transfer Coefficient and Temperature Profile

The heat-transfer coefficient and temperature profile are calculated in the same way as the friction coefficient and velocity profile. The expression for the heat transfer by conduction in a direction normal to the wall in a laminar flow is

$$q = -\kappa \frac{\partial T}{\partial y} \tag{22}$$

It is assumed that an eddy thermal diffusivity exists that allows the heat transfer in a turbulent flow to be written as

$$q = -(\kappa + \rho c_p \epsilon_h) \frac{\partial T}{\partial y} \tag{23}$$

Equation (23) can be written as

$$q = -\kappa \left[1 + \left(\frac{\epsilon_m}{\nu}\right)\left(\frac{\epsilon_h}{\epsilon_m}\right) Pr\right] \frac{\partial T}{\partial y} \tag{24}$$

After defining a non-dimensional temperature t by

$$t = \frac{T - T_w}{T_e - T_w} ,$$

introducing a temperature boundary-layer thickness δ_T, and dividing by q_w, (24) becomes

$$\frac{q}{q_w} = -\frac{\kappa (T_e - T_w)}{\delta_T q_w} \left[1 + \left(\frac{\epsilon_m}{\nu}\right)\left(\frac{\epsilon_h}{\epsilon_m}\right) Pr\right] \frac{\partial t}{\partial \eta_T} \tag{25}$$

where $\eta_T = \frac{y}{\delta_T}$. After introduction of the Stanton number

$$S_t = -\frac{q_w}{\rho u_e c_p (T_e - T_w)} ,$$

equation (25) becomes

$$\frac{q}{q_w} = \frac{1}{S_t Re_\delta \left(\frac{\delta_T}{\delta}\right) Pr} \left[1 + \left(\frac{\epsilon_m}{\nu}\right)\left(\frac{\epsilon_h}{\epsilon_m}\right) Pr\right] \frac{\partial t}{\partial \eta_T} \tag{26}$$

From (26) it follows that

$$S_t Re_\delta \left(\frac{\delta_T}{\delta}\right) Pr \int_0^1 \frac{\frac{q}{q_w}\, d\eta_T}{1+\left(\frac{\epsilon_m}{\nu}\right)\left(\frac{\epsilon_h}{\epsilon_m}\right)Pr} = \int_0^1 \frac{\partial t}{\partial \eta_T} d\eta_T = 1 \qquad (27)$$

or

$$\frac{1}{S_t Re_\delta Pr} = \frac{\delta_T}{\delta} \int_0^1 \frac{\frac{q}{q_w}}{1+\left(\frac{\epsilon_m}{\nu}\right)\left(\frac{\epsilon_h}{\epsilon_m}\right)Pr}\, d\eta_T \qquad (28)$$

Before (28) can be used to calculate S_t the ratio $\frac{q}{q_w}$ must be known as a function of η_T. Unlike $\frac{\tau}{\tau_w}$, no measurements of $\frac{q}{q_w}$ on a plate could be found. Consequently, to obtain an approximate distribution of $\frac{q}{q_w}$, the Fediaevsky method for getting $\frac{\tau}{\tau_w}$ was used to investigate the dependence of $\frac{q}{q_w}$ on η_T. This method gave a reasonable approximation to $\frac{\tau}{\tau_w}$ (see fig. 1). Two conditions to evaluate the fourth degree polynomial of Fediaevsky's method are

$$\frac{q}{q_w} = 1 \quad \text{at} \quad y = 0$$

and

$$\frac{q}{q_w} = 0 \quad \text{at} \quad y = \delta_T$$

Also, from the energy equation,

$$\rho u \frac{\partial E}{\partial x} + \rho v \frac{\partial E}{\partial y} = -\frac{\partial q}{\partial y} \qquad (29)$$

and the conditions, $v_w = 0$ and $\left(\frac{\partial E}{\partial x}\right)_w = 0$, it follows that both

$$\frac{\partial}{\partial y}\left(\frac{q}{q_w}\right) = 0 \quad \text{and} \quad \frac{\partial^2}{\partial y^2}\left(\frac{q}{q_w}\right) = 0 \quad \text{at} \quad y = 0 .$$

Moreover, for $\left(\frac{\partial E}{\partial x}\right)_e = 0$, the condition at $y = \delta_T$ is

$$\frac{\partial}{\partial y}\left(\frac{q}{q_w}\right) = 0 .$$

These five conditions on $\frac{q}{q_w}$ are exactly the same as on $\frac{\tau}{\tau_w}$. Consequently, if $\frac{\tau}{\tau_w}$ and $\frac{q}{q_w}$ are approximated by fourth degree polynomials $\frac{q}{q_w}$ is exactly the same function of η_T as $\frac{\tau}{\tau_w}$ is of η. Therefore, the relation between $\frac{q}{q_w}$ and η_T is assumed to be the same as the experimental one between $\frac{\tau}{\tau_w}$ and η. Actually, however, $\frac{q}{q_w}$ depends slightly on the Prandtl number (see fig. 7-55, ref. (1)).

In figure 11 is shown the connection between Re_θ and Re_x calculated by use of (20). Figure 11 is given because it enables quantities known as a function of Re_θ to be easily obtained as a function of Re_x and vice versa. Thus, from this figure and figure 9 the dependence of $C_f/2$ on Re_x can be found.

Heat-Transfer Coefficient and Temperature Profile

The heat-transfer coefficient and temperature profile are calculated in the same way as the friction coefficient and velocity profile. The expression for the heat transfer by conduction in a direction normal to the wall in a laminar flow is

$$q = -K \frac{\partial T}{\partial y} \tag{22}$$

It is assumed that an eddy thermal diffusivity exists that allows the heat transfer in a turbulent flow to be written as

$$q = -(K + \rho c_p \epsilon_h) \frac{\partial T}{\partial y} \tag{23}$$

Equation (23) can be written as

$$q = -K \left[1 + \left(\frac{\epsilon_m}{\nu}\right)\left(\frac{\epsilon_h}{\epsilon_m}\right) Pr\right] \frac{\partial T}{\partial y} \tag{24}$$

After defining a non-dimensional temperature t by

$$t = \frac{T - T_w}{T_e - T_w} ,$$

introducing a temperature boundary-layer thickness δ_T, and dividing by q_w, (24) becomes

$$\frac{q}{q_w} = -\frac{K(T_e - T_w)}{\delta_T q_w} \left[1 + \left(\frac{\epsilon_m}{\nu}\right)\left(\frac{\epsilon_h}{\epsilon_m}\right) Pr\right] \frac{\partial t}{\partial \eta_T} \tag{25}$$

where $\eta_T = \frac{y}{\delta_T}$. After introduction of the Stanton number

$$S_t = -\frac{q_w}{\rho u_e c_p (T_e - T_w)} ,$$

equation (25) becomes

$$\frac{q}{q_w} = \frac{1}{S_t Re_\delta \left(\frac{\delta_T}{\delta}\right) Pr} \left[1 + \left(\frac{\epsilon_m}{\nu}\right)\left(\frac{\epsilon_h}{\epsilon_m}\right) Pr\right] \frac{\partial t}{\partial \eta_T} \tag{26}$$

From (26) it follows that

$$S_t Re_\delta \left(\frac{\delta_T}{\delta}\right) Pr \int_0^1 \frac{\frac{q}{q_w}\, d\eta_T}{1+\left(\frac{\epsilon_m}{\nu}\right)\left(\frac{\epsilon_h}{\epsilon_m}\right)Pr} = \int_0^1 \frac{\partial t}{\partial \eta_T}\, d\eta_T = 1 \qquad (27)$$

or

$$\frac{1}{S_t Re_\delta Pr} = \frac{\delta_T}{\delta} \int_0^1 \frac{\frac{q}{q_w}}{1+\left(\frac{\epsilon_m}{\nu}\right)\left(\frac{\epsilon_h}{\epsilon_m}\right)Pr}\, d\eta_T \qquad (28)$$

Before (28) can be used to calculate S_t the ratio $\frac{q}{q_w}$ must be known as a function of η_T. Unlike $\frac{\tau}{\tau_w}$, no measurements of $\frac{q}{q_w}$ on a plate could be found. Consequently, to obtain an approximate distribution of $\frac{q}{q_w}$, the Fediaevsky method for getting $\frac{\tau}{\tau_w}$ was used to investigate the dependence of $\frac{q}{q_w}$ on η_T. This method gave a reasonable approximation to $\frac{\tau}{\tau_w}$ (see fig. 1). Two conditions to evaluate the fourth degree polynomial of Fediaevsky's method are

$$\frac{q}{q_w} = 1 \quad \text{at} \quad y = 0$$

and

$$\frac{q}{q_w} = 0 \quad \text{at} \quad y = \delta_T$$

Also, from the energy equation,

$$\rho u \frac{\partial E}{\partial x} + \rho v \frac{\partial E}{\partial y} = \frac{-\partial q}{\partial y} \qquad (29)$$

and the conditions, $v_w = 0$ and $\left(\frac{\partial E}{\partial x}\right)_w = 0$, it follows that both

$$\frac{\partial}{\partial y}\left(\frac{q}{q_w}\right) = 0 \quad \text{and} \quad \frac{\partial^2}{\partial y^2}\left(\frac{q}{q_w}\right) = 0 \quad \text{at} \quad y = 0 .$$

Moreover, for $\left(\frac{\partial E}{\partial x}\right)_e = 0$, the condition at $y = \delta_T$ is

$$\frac{\partial}{\partial y}\left(\frac{q}{q_w}\right) = 0 .$$

These five conditions on $\frac{q}{q_w}$ are exactly the same as on $\frac{\tau}{\tau_w}$. Consequently, if $\frac{\tau}{\tau_w}$ and $\frac{q}{q_w}$ are approximated by fourth degree polynomials $\frac{q}{q_w}$ is exactly the same function of η_T as $\frac{\tau}{\tau_w}$ is of η. Therefore, the relation between $\frac{q}{q_w}$ and η_T is assumed to be the same as the experimental one between $\frac{\tau}{\tau_w}$ and η. Actually, however, $\frac{q}{q_w}$ depends slightly on the Prandtl number (see fig. 7-55, ref. (1)).

The Prandtl number also affects the ratio $\frac{\delta_T}{\delta}$ in equation (23). Thus, for laminar flow over a flat plate

$$\frac{\delta_T}{\delta} = Pr^{-\frac{1}{3}} \qquad \text{(p. 323 ref. 2)}$$

For Pr = .738, the value used in the present analysis, this relation gives 1.106 for $\frac{\delta_T}{\delta}$. For turbulent flow $\frac{\delta_T}{\delta}$ is probably smaller and so, as an allowable approximation, is taken as unity. Equation (23) then becomes

$$\frac{1}{S_t Re_\delta Pr} = \int_0^1 \frac{\frac{q}{q_w}}{1+\left(\frac{\epsilon_m}{\nu}\right)\left(\frac{\epsilon_h}{\epsilon_m}\right)Pr}\, d\eta \tag{30}$$

For reasons given in the section, "Friction Coefficient and Velocity Profiles," (30) is written as

$$\frac{1}{S_t Re_\delta Pr} = \frac{1}{Re_f}\int_0^{y_{+,2}} \frac{\frac{q}{q_w}}{1+\frac{\epsilon_h}{\epsilon_m} y_+ f_1 Pr}\, dy_+ + \int_{\eta_2}^1 \frac{\frac{q}{q_w}}{1+\frac{\epsilon_h}{\epsilon_m} Re_f f_2 Pr}\, d\eta \tag{31}$$

The values $y_{+,2}$ and η_2 are permitted to differ from $y_{+,1}$ and η_1.

To find the ratio of the eddy thermal diffusivity to the eddy kinematic viscosity, $\frac{\epsilon_h}{\epsilon_m}$, the pipe flow data of reference (3) were used. First, the values of $\frac{\epsilon_h}{u_* r}$ given in reference (3) for five Reynolds numbers at each of twelve values of y/r were averaged. This was allowable because there was no consistent effect of Reynolds number on $\frac{\epsilon_h}{u_* r}$ at the twelve stations. A smooth curve of $\frac{\epsilon_h}{u_* r}$ against y/r was then drawn through these average values located at the twelve values of y/r. Then a curve of $\frac{\epsilon_m}{u_* r}$ for pipe flow was obtained by first averaging Laufer's and Nunner's data given in figure 7-39 of reference (1) at each of 3 values of y/r and then drawing a smooth curve through the average values. Laufer's and Nunner's data are the same from the wall to the position of the maximum in $\frac{\epsilon_m}{u_* r}$ but Laufer's data are slightly higher beyond this point. Although Re_f is estimated to be about 6.3×10^3 for Laufer's data and about 6.6×10^2 for Nunner's data, a ratio of about 9.5, it is not certain that this is the reason for the difference. At each value of y/δ or y/r, the ratio $\left(\frac{\epsilon_m}{u_* \delta}\right)\Big/\left(\frac{\epsilon_m}{u_* r}\right)$ was then calculated with the help of figure 2. This ratio was calculated because the eddy kinematic viscosity approaches zero at the outer edge of a boundary layer, whereas, it does not at the center of a pipe. The ratio $\left(\frac{\epsilon_m}{u_* \delta}\right)\Big/\left(\frac{\epsilon_m}{u_* r}\right)$ was plotted against y/δ and a smooth curve drawn through the plotted values. The assumption was then made that a change in flow from pipe to

plate has the same effect on ϵ_h as it does on ϵ_m. Therefore, $\frac{\epsilon_h}{u_\tau \delta}$ was obtained by multiplying the ordinates of the curve for $\frac{\epsilon_h}{u_\tau r}$ obtained from the pipe flow data of reference (3) by $\left(\frac{\epsilon_m}{u_\tau \delta}\right)\Big/\left(\frac{\epsilon_m}{u_\tau r}\right)$. The variation of $\frac{\epsilon_h}{\epsilon_m}$ with y/δ for plate flow was then calculated and is shown in figure 12. For $\eta \lesssim .06$, $\frac{\epsilon_h}{\epsilon_m}$ is taken as unity. This means that $\frac{\epsilon_h}{u_\tau \delta}$ is assumed to be $f_2(\eta)$ for $\eta \lesssim .06$ with the result that

$$\frac{\epsilon_h}{u_\tau \delta} = .393\eta \qquad (\eta \lesssim .06)$$

Consequently, $\frac{\epsilon_h}{u_\tau y}$ as a function of y_+ has a horizontal portion

$$\frac{\epsilon_h}{u_\tau y} = .393$$

just as $\frac{\epsilon_m}{u_\tau y}$ has.

Near the wall the proper variable is y_+ instead of η. For this region the data of references (6) and (7) for flow of air in a channel were used to obtain the connection between $\frac{\epsilon_h}{u_\tau y}$ and y_+. The values of $\frac{\epsilon_h}{u_\tau y}$ and y_+ were calculated by using $\rho = 22 \times 10^{-4}$ slugs per cubic foot and $\nu = 1.8 \times 10^{-4}$ square feet per second. The results are shown in figure 13 for the entire range of y_+ from the wall to the center line of the channel. Where $\frac{\epsilon_h}{u_\tau y}$ is a function of y_+ the data fall almost on f_1, except perhaps between about 3 and 17 where the $\frac{\epsilon_h}{u_\tau y}$ data lie somewhat below f_1. The agreement between these $\frac{\epsilon_h}{u_\tau y}$ data and f_1 is believed to be sufficiently close to allow f_1 to represent $\frac{\epsilon_h}{u_\tau y}$ as well as $\frac{\epsilon_m}{u_\tau y}$. This means that $\frac{\epsilon_h}{\epsilon_m} = 1$ near the wall where the distance variable is y_+ instead of η.

The value of $y_{+,2}$ and the corresponding value of η_2 in (31) are calculated in the same way as $y_{+,1}$ and η_1. To do this, figures 2 and 12 are used to calculate $\left(\frac{\epsilon_m}{u_\tau y}\right)\left(\frac{\epsilon_h}{\epsilon_m}\right)$ as a function of y_+ by use of (9) and (11). The value of y_+ at which $\left(\frac{\epsilon_m}{u_\tau y}\right)\left(\frac{\epsilon_h}{\epsilon_m}\right)$ equals f_1 is then found. Below this value of y_+, called $y_{+,2}$, $\frac{\epsilon_h}{u_\tau y}$ is represented by f_1; above $y_{+,2}$ figures 2 and 12 are used to get $\left(\frac{\epsilon_m}{u_\tau y}\right)\left(\frac{\epsilon_h}{\epsilon_m}\right)$ as a function of η. In Table V are given the values of $y_{+,2}$ and η_2 for the three values of Re_f for which $y_{+,2}$ is less than 52.

The data in figure 13 indicate that the assumption that there is a quantity $y_{+,1}$ or $y_{+,2}$ seems to be correct. The method for the calculation of $y_{+,1}$ or $y_{+,2}$ also appears correct. That is, the data show that below the intersection of $\frac{\epsilon_h}{\epsilon_m}$ $f_2(\eta)$ with

$f_1(y_+)$, $\frac{\epsilon_h}{u_\infty y}$ depends on y_+. Above the intersection, $\frac{\epsilon_h}{u_\infty y}$ depends on y_+ and on Re_f. That is, above the intersection the variable is $\frac{\epsilon_h}{u_\infty \delta}$ and it depends on n. As expected, there is a smooth transition between f_1 and $\frac{\epsilon_h}{\epsilon_m} f_2$ rather than the corner that results in the present method for finding $y_{+,1}$ and $y_{+,2}$. For Re_f = 150 and 264, the experimental data leave f_1 close to the calculated value of $y_{+,2}$. For Re_f = 701, there is an appreciable difference. Above $y_{+,2}$ the calculated curves for all three values of Re_f are below the experimental data. Because the calculated curves are for flow over a plate whereas the points are for a channel, some difference is to be expected. Thus, although the value of $\frac{\epsilon_h}{u_\infty y}$ for a plate approaches zero at the outer edge of the boundary layer, the value of $\frac{\epsilon_h}{u_\infty y}$ for a channel is not zero at the center line. This is why the dashed curves in figure 13 go through $\frac{\epsilon_h}{u_\infty y} = 0$ at $y_+ = Re_f$, but the points do not. For $y_{+,1} < y_+ < Re_f$, but not close to $y_+ = Re_f$, only a small part of the difference between the curves and the data points can be removed by multiplying $\frac{\epsilon_h}{u_\infty y}$ for plate flow by the reciprocal of the ratio $\left(\frac{\epsilon_m}{u_\infty \delta}\right)/\left(\frac{\epsilon_m}{u_\infty r}\right)$ that was used to convert the pipe flow $\left(\frac{\epsilon_h}{u_\infty r}\right)$ data of reference (3) to plate flow $\frac{\epsilon_h}{u_\infty \delta}$ data. The reason for the remaining difference is not clear at present.

By use of equation (31), the function f_1, figures 2 and 12, and the method for finding $y_{+,2}$, the local Stanton number, S_t, was calculated for the five values of Re_f listed in Table I. The results are given in Table VI and also shown in figure 9 as a function of Re_θ. Also given in Table VI and figure 14 are the values of the ratio $\frac{2S_t}{c_f}$.

The ratio $\frac{2S_T}{C_F}$ was calculated by noting that from the definition of S_T and of S_t it follows that

$$S_T = \frac{1}{Re_x} \int_0^{Re_x} S_t \, dRe_x \tag{32}$$

or

$$S_T = \frac{1}{Re_x} \int_0^{Re_\theta} S_t \frac{dRe_x}{dRe_\theta} \, dRe_\theta \tag{33}$$

Upon the use of (19) and (21), (33) becomes

$$\frac{2S_T}{C_F} = \frac{1}{Re_\theta}\int_0^{Re_\theta}\frac{2S_t}{C_f}\,dRe_\theta \tag{34}$$

For $0 < Re_\theta < 100$, the ratio $\frac{2S_t}{C_f}$ was expressed in an analytic form by assuming that

$$S_t = \frac{k_1}{Re_\theta^{n_1}} \tag{35}$$

The constants k_1 and n_1 were determined from the values of S_t for Re_θ equal to 27.7 and 191 (see Table VI) and were found to equal .109 and .601, respectively. When the results for k_o and n_o are used, the expression for $\frac{2S_t}{C_f}$ for $Re_\theta < 100$ becomes

$$\frac{2S_t}{C_f} = \frac{1.381}{Re_\theta^{.0225}} \tag{36}$$

Equation (36) was used with (34) to obtain $\frac{2S_T}{C_F} = 1.274$ for $Re_\theta = 100$. For values of Re_θ larger than 100, $\frac{2S_T}{C_F}$ was calculated by numerical integration by use of (34) and figure (14). The result is shown in figure (14).

The temperature profiles were calculated by putting $\frac{\delta_T}{\delta} = 1$, solving (26) for $\frac{dt}{d\eta}$, and integrating between 0 and η. Thus,

$$t = S_t Re_\delta Pr\int_0^\eta \frac{\frac{q}{q_w}}{1+\left(\frac{\epsilon_m}{\nu}\right)\left(\frac{\epsilon_h}{\epsilon_m}\right)Pr}\,d\eta \tag{37}$$

or

$$t = \frac{S_t Pr}{\sqrt{\frac{C_f}{2}}}\int_0^{y_{t,2}}\frac{\frac{q}{q_w}}{1+y_t f_1 Pr}\,dy_t + S_t Re_\delta Pr\int_{\eta_2}^\eta \frac{\frac{q}{q_w}}{1+\frac{\epsilon_h}{\epsilon_m}f_2 Re_f Pr}\,d\eta \tag{38}$$

The temperature profiles calculated by use of (38) are shown in figure 15 and tabulated in Table VII. Also shown is the temperature profile for laminar flow. This profile is obtained by letting $\left(\frac{\epsilon_m}{\nu}\right) = 0$ and $\frac{q}{q_w} = \frac{\tau}{\tau_w}$ in (37). The result is

$$t = S_t Re_\delta Pr\int_0^\eta \frac{\tau}{\tau_w}\,d\eta$$

or, after using (17)

$$t = \frac{2S_t Pr}{C_f}\,\phi \tag{39}$$

From (30) with $\left(\frac{q}{q_w}\right) = \left(\frac{\tau}{\tau_w}\right)$ and $\left(\frac{\epsilon_m}{\nu}\right) = 0$, and from (16) it follows that

$$\frac{2 S_t Pr}{c_f} = 1$$

Therefore, from (39) $t = \phi$. That is, the present method predicts that for laminar flow the velocity and temperature profiles are the same.

Mass-Transfer Coefficient and Concentration Profile

The mass-transfer coefficient and concentration profile are calculated in the same way as the heat-transfer coefficient and temperature profile. For a binary mixture in laminar flow the mass transfer by diffusion in the direction normal to the wall is,

$$m_1 = -\rho \mathcal{D}_{12} \frac{\partial c_1}{\partial y} - \frac{D_T}{T} \frac{\partial c_1}{\partial y} \tag{40}$$

where the contribution of $\frac{D_T}{T} \frac{\partial c_1}{\partial y}$ is assumed to be negligible. For turbulent flow it is assumed that an eddy diffusivity exists such that

$$m_1 = -\rho \left(\mathcal{D}_{12} + \epsilon_d\right) \frac{\partial c_1}{\partial y} \tag{41}$$

After introduction of the Schmidt number $\frac{\mu}{\rho \mathcal{D}_{12}}$, and the quantity

$$\xi = \frac{c_1 - c_{1w}}{c_{1e} - c_{1w}}$$

equation (41) becomes

$$m_1 = -\rho \mathcal{D}_{12} \left[1 + \left(\frac{\epsilon_m}{\nu}\right)\left(\frac{\epsilon_d}{\epsilon_m}\right) S_c\right] \frac{c_{1e} - c_{1w}}{\delta} \frac{\partial \xi}{\partial \eta} \tag{42}$$

In the same way as in the section concerning heat transfer, it is assumed here that the concentration boundary layer thickness differs from the velocity boundary layer thickness by less than 10 percent and that it is thus permissible to take the two thicknesses equal.

When (42) is divided through by $m_{1,w}$ and the mass-transfer coefficient

$$c_m = \frac{-m_{1w}}{\rho u_e (c_{1e} - c_{1w})} \tag{43}$$

is introduced, the result is

$$\frac{m_1}{m_{1w}} = \frac{1}{c_m Re_\delta S_c} \left[1 + \left(\frac{\epsilon_m}{\nu}\right)\left(\frac{\epsilon_d}{\epsilon_m}\right) S_c\right] \frac{\partial \xi}{\partial \eta} \tag{44}$$

From (44) it follows that

$$c_m Re_\delta S_c \int_0^1 \frac{\frac{m_1}{m_{1w}}}{1 + \left(\frac{\epsilon_m}{\nu}\right)\left(\frac{\epsilon_d}{\epsilon_m}\right) S_c} d\eta = \int_0^1 \frac{\partial \xi}{\partial \eta} d\eta = 1 \tag{45}$$

or

$$\frac{1}{C_m Re_\delta S_c} = \int_0^1 \frac{\frac{m_1}{m_{1w}}}{1+\left(\frac{\epsilon_m}{\nu}\right)\left(\frac{\epsilon_d}{\epsilon_m}\right)S_c}\, d\eta \qquad (46)$$

Information concerning $\frac{m_1}{m_{1w}}$ as a function of η is obtained by noting that

$$\frac{m_1}{m_{1w}} = 1 \quad \text{at} \quad y = 0$$

and

$$\frac{m_1}{m_{1w}} = 0 \quad \text{at} \quad y = \delta$$

Moreover, from the diffusion equation

$$\rho u \frac{\partial c_1}{\partial x} + \rho v \frac{\partial c_1}{\partial y} = -\frac{\partial m_1}{\partial y} \qquad (47)$$

it follows that

$$\left(\frac{\partial m_1}{\partial y}\right)_w = 0$$

when the diffusion velocity is small enough for $v_w = 0$.

If, in addition, $\left(\frac{\partial c_1}{\partial x}\right)_w = 0$ and $\left(\frac{\partial c_1}{\partial x}\right)_e = 0$, then also

$$\left(\frac{\partial^2 m_1}{\partial y^2}\right)_w = 0$$

and

$$\left(\frac{\partial m_1}{\partial y}\right)_\delta = 0$$

Because these boundary conditions are the same as those for $\frac{q}{q_w}$, it is assumed that the non-dimensional concentration distribution is the same as the non-dimensional heat-transfer distribution. It is also assumed that $\frac{\epsilon_d}{\epsilon_h} = 1$ and that $S_c = Pr$. From these assumptions it follows that

$$C_m = S_t$$

Moreover, the non-dimensional concentration profile is then also the same as the non-dimensional temperature profile. If either $\frac{\epsilon_d}{\epsilon_h} \neq 1$ or $S_c \neq Pr$, the method used to calculate the heat transfer coefficient and temperature profile can be used to calculate the mass-transfer coefficient and concentration profile.

DISCUSSION

Friction Coefficient and Velocity Profile

One of the methods for obtaining the logarithmic friction formula and velocity profile is Millikan's method of overlap.

In this method it is shown that if there is a region of the boundary layer in which

$$u_+ = f_3(y_+)$$

and

$$\frac{u_e - u}{u_*} = f_4(\eta)$$

are both valid, then the friction formula is the logarithmic one and the velocity profile is logarithmic in the region of overlap.

In the present analysis the logarithmic friction formula and velocity profile also follow from an overlap condition. Here, however, the condition is on the eddy kinematic viscosity instead of on velocity profile functions. Thus, to obtain a friction formula for large Reynolds numbers equation (10) is used. For large Reynolds numbers

$$y_{+,1} = 52$$

and

$$\eta_1 = \frac{52}{Re_f}$$

The value of η_1 is thus very small. Consequently, $\frac{\tau}{\tau_w}$ is almost unity for $y_+ \leq 52$. Moreover, the indication from figure 1 is that $\frac{\tau}{\tau_w}$ is practically unity for η less than about .01. In addition, for large enough values of Re_f, equation (12) applies for a range of η that begins at $52/Re_f$ and extends outward at least as far as .01. Equation (10) then becomes

$$\frac{1}{\sqrt{\frac{c_f}{2}}} = \int_0^{52} \frac{dy_+}{1 + y_+ f_1} + Re_f \int_{\frac{52}{Re_f}}^{.01} \frac{d\eta}{1 + \kappa \eta Re_f} + Re_f \int_{.01}^{1} \frac{\frac{\tau}{\tau_w}\, d\eta}{1 + Re_f f_2} \qquad (48)$$

For large Re_f the quantity $(1 + Re_f f_2)$ in the last term of (48) is almost equal to $Re_f f_2$ except very close to $\eta = 1$. For example, at $Re_f = 5 \times 10^5$, $Re_f f_2 = 1965$ at $\eta = .01$. It then increases to about 34,000 at $\eta = .31$ and decreases to zero at $\eta = 1$; at $\eta = .98$, however, it is equal to 850. For large Reynolds numbers the last term in (48) can be written as

$$\int_{.01}^{1-\Delta} \frac{\frac{\tau}{\tau_w}}{f_2}\, d\eta + Re_f \int_{1-\Delta}^{1} \frac{\frac{\tau}{\tau_w}}{1 + Re_f f_2}\, d\eta$$

where $(1-\Delta)$ is the upper limit of the range of η in which $Re_f f_2$ is much larger than unity. As Re_f increases, Δ decreases and

$$Re_f \int_{1-\Delta}^{1} \frac{\frac{\tau}{\tau_w}}{1 + Re_f f_2}\, d\eta$$

becomes negligible. For large Re_f the last term in (48) is then approximately independent of Re_f. Its value is 14.27. The first term in (48) has the value 13.94. When these two numerical values are used and the second term of (48) is integrated analytically, the result is

$$\frac{1}{\sqrt{\frac{C_f}{2}}} = 28.21 + \frac{1}{K}\ln(1+.01K\,Re_f) - \frac{1}{K}\ln(1+52K) \qquad (49)$$

For large Reynolds numbers

$$\ln(1+.01K\,Re_f) \approx \ln(.01K\,Re_f)$$

Equation (49) then becomes

$$\frac{1}{\sqrt{\frac{C_f}{2}}} = 2.54\ln Re_f + 6.31 \qquad (K=.393) \qquad (50)$$

Note that the logarithmic form requires only that there be a region of the boundary layer, no matter how small, in which (12) and $\frac{\tau}{\tau_w} \cong 1$ are both valid.

Equation (50) has the form of von Karman's friction formula (ref. (8)). Although (50) was derived for very large Reynolds numbers the value of $C_f/2$ obtained from it differs from the value given in Table II by less than 2 percent for $Re_f = 2960$.

By writing (50) in the form

$$\frac{1}{\sqrt{\frac{C_f}{2}}} = 2.54\ln\sqrt{\frac{C_f}{2}}\,Re_\theta + 2.54\ln\frac{\delta}{\theta} + 6.31$$

and using the value of $\frac{\delta}{\theta}$ for $Re_f = 5 \times 10^5$ from Table IV, there is obtained the relation

$$\frac{1}{\sqrt{\frac{C_f}{2}}} = 2.54\ln\sqrt{\frac{C_f}{2}}\,Re_\theta + 12.77 \qquad (51)$$

The value of $C_f/2$ obtained from (51) differs from that in Table II by almost 7 percent for $Re_f = 2960$. Equation (51) has larger errors than (50) at small Reynolds numbers because the ratio $\left(\frac{\delta}{\theta}\right)$ depends on Reynolds number (see Table IV) and the value of $\left(\frac{\delta}{\theta}\right)$ for $Re_f = 5 \times 10^5$ was used to get (51). Because formulas of the logarithmic type are inconvenient for computation, it is usually better either to use the curves of figures 9 or 10 or convenient approximations.

The friction coefficient was calculated for turbulent flow over the entire range of Reynolds number by use of the one non-dimensional shear distribution shown in figure 1. The good agreement between the friction coefficient calculated by the present method and the accepted friction coefficient (see figs. 5 and 10) indicates that the non-dimensional shear distribution is approximately independent of Reynolds number. Moreover, when the value of $\frac{\delta}{\theta}$ is calculated for the laminar velocity profile, and substituted into (16), the result is

$$\frac{C_f}{2} = \frac{.2258}{Re_\theta} \tag{52}$$

This expression differs from the exact one

$$\frac{C_f}{2} = \frac{.2205}{Re_\theta} \tag{53}$$

by less than 2 1/2 percent. Because (52) was obtained by use of the same shear distribution as was used for turbulent flow, the inference is that the non-dimensional shear distribution on a flat plate is approximately the same for laminar as for turbulent flow. Fediaevsky's method (ref. (4)) predicts them to be identical.

In contrast to the usual method in which the velocity profiles are calculated by patching the results of a number of approaches, each yielding a portion of the velocity profile, the present analysis calculates the entire velocity profile by one approach. Moreover, the present method yields many of the results that are presently accepted. For example, in the region very close to the wall equation (14) applies. Here $f_1 \ll 1$ and $\frac{\tau}{\tau_w} \cong 1$. Then (14) becomes

$$\phi = \sqrt{\frac{c_f}{2}} \int_0^{y_+} dy_+$$

or

$$u_+ = y_+ \tag{54}$$

This is the well-known velocity profile of the laminar sublayer (ref. (1)).

From equations (1) and (2) it follows that the ratio of the turbulent shear, $\rho \epsilon_m \frac{\partial u}{\partial y}$, to the laminar shear, $\mu \frac{\partial u}{\partial y}$, is $\frac{\epsilon_m}{\nu}$, or $y_+ f_1$. The value of unity for this ratio has often been suggested as a criterion for the edge of the laminar sublayer. By use of figure 3 it is found that this ratio is equal to unity when y_+ is about 9.9, a value in the range of accepted values for the outer edge of the laminar sublayer.

For somewhat larger values of y_+ the ratio $\frac{\tau}{\tau_w}$ is still approximately equal to unity if Re_f is sufficiently large.

Then (14) becomes

$$\phi = \sqrt{\frac{c_f}{2}} \int_0^{y_+} \frac{dy_+}{f_5(y_+)}$$

or

$$u_+ = f_6(y_+) \tag{55}$$

Equation (55) is the law of the wall (ref. (1)). Its upper limit is either the upper limit for f_1 or for $\frac{\tau}{\tau_w} \approx 1$, whichever value of y_+ is smaller.

When Re_δ is large enough for a region of overlap to exist, equation (12) is valid for a range of η whose upper limit is near .06 (see figure 2). Equation (15) then becomes

$$\phi = \sqrt{\frac{c_f}{2}} \int_0^{52} \frac{\frac{\tau}{\tau_w}}{1+y_+ f_1} dy_+ + \frac{c_f}{2} Re_\delta \int_{\frac{52}{Re_f}}^{\eta} \frac{\frac{\tau}{\tau_w}}{1+K\eta Re_f} d\eta \qquad \left(\frac{52}{Re_f} \leq \eta \approx .06\right) \tag{56}$$

For large enough Re_δ the range in which τ/τ_w is almost unity extends from the wall to a value of η greater than $52/Re_\delta$. Thus, at $\eta = .06$, which is greater than $52/Re_\delta$ when Re_δ is large, $\frac{\tau}{\tau_w} = .992$. Therefore, take $\frac{\tau}{\tau_w} = 1$ in (56). Then (56) becomes

$$\phi = \sqrt{\frac{c_f}{2}} \left\{ \int_0^{52} \frac{dy_+}{1+y_+ f_1} + \frac{\frac{c_f}{2} Re_\delta}{K Re_f} \ln\left[1+K\eta Re_f\right] \right\}_{\frac{52}{Re_f}}^{\eta}$$

or

$$\frac{\phi}{\sqrt{\frac{c_f}{2}}} = 13.94 + \frac{1}{K} \ln\left(1+K\eta Re_f\right) - \frac{1}{K} \ln\left(1+52K\right) \qquad \left(\frac{52}{Re_f} \leq \eta \approx .06\right) \tag{57}$$

The smallest value of $(1 + K\eta Re_f)$ is $(1 + 52K)$. But $\ln(1 + 52K)$ differs from $\ln 52K$ by less than one percent for $K = .393$. Consequently, (57) can be written as

$$\frac{\phi}{\sqrt{\frac{c_f}{2}}} = 13.94 + \frac{1}{K} \ln K\eta Re_f - \frac{1}{K} \ln 52K$$

or as

$$u_+ = 2.54 \ln\eta + 2.54 \ln Re_f + 3.89 \qquad \left(\frac{52}{Re_f} \leq \eta \approx .06\right) \tag{58}$$

Equation (58) is the logarithmic profile.

Equation (58) was obtained by requiring that $\frac{\tau}{\tau_w} \cong 1$ and that (12) both apply. Consequently, it would seem that the profile should not be logarithmic for $\eta \gtrsim .06$ or so; $\eta = .06$ is roughly the upper limit for (12). When, however, (9) is used with figure 7 it is found that the velocity profiles do not differ noticeably from the logarithmic profile unless η is much larger than .06. For example, the values of η for departure from the logarithmic profile vary from about .17 for $Re_f = 2960$ to about .20 for $Re_f = 5 \times 10^5$. For Re_f equal to 200 there appears to be very little, if any, logarithmic portion in figure 7; the lower values of Re_f definitely have none. The velocity profiles thus have a logarithmic appearing portion for values of η larger than a strict application of the requirements indicate. The reason for this behavior is probably the slow decrease of $\frac{\epsilon_m}{u_* \delta}$ from $K\eta$ (see fig. 2) combined with the slow decrease of $\frac{\tau}{\tau_w}$ from unity for η less than about .2 (see fig. 1).

As the Reynolds number decreases, the value of η_1, which for large Reynolds numbers is equal to $\frac{52}{Re_f}$, increases. The increase in η_1 decreases the range of η for which (12) is valid and, as a result, decreases the extent of the logarithmic portion of the velocity profile. If the upper limit of (12) is taken at $\eta \cong .06$ (see fig. 2), there will be no logarithmic portion of the velocity profile when Re_f becomes less than 867. At this value of Re_f, η_1 exceeds .06. The value 867 for Re_f corresponds to a value of 2000 for Re_θ. Note that the lower limit for the logarithmic velocity profile is also the lower limit for the logarithmic friction formula, equation (50).

Although, strictly speaking, there is no logarithmic portion of the velocity profile for $Re_f < 867$, the discussion concerning the extent of the logarithmic profile indicated that according to figure 7 a velocity profile has a logarithmic appearing portion down to Re_f in the neighborhood of 200. For $Re_f = 200$, Re_θ is about 450. Preston (ref. (9)) took the lower edge of the logarithmic portion of the profile at $y_+ = 30$ and the upper edge at $\eta = .20$ and found that the extent of the logarithmic portion shrank to zero at $Re_f = 150$. From this value, Preston obtained 389 for the value of Re_θ below which there is no logarithmic portion of the velocity profile. From figure 3 it seems that 30 is too small a value of y_+ for the logarithmic profile to hold. Here again, however, the velocity profile departs slowly from the logarithmic type (see also ref. (10)) so that it has the logarithmic appearance for smaller values of y_+ than is to be expected.

Beyond the logarithmic portion of the velocity profile lies the region of the velocity defect formula (ref. (1)). To obtain this formula from the present analysis, equation (15) is written for $\eta = 1$, thus,

$$1 = \sqrt{\frac{c_f}{2}} \int_0^{y_{+,1}} \frac{\frac{\tau}{\tau_w}}{1 + y_+ f_1} dy_+ + \frac{c_f}{2} Re_\delta \int_{\eta_1}^{1} \frac{\frac{\tau}{\tau_w}}{1 + Re_f f_2} d\eta \tag{59}$$

When (15) is subtracted from (59), the result is

$$1 - \phi = \frac{c_f}{2} Re_\delta \int_\eta^1 \frac{\frac{\tau}{\tau_w}}{1 + Re_f f_2} d\eta$$

or

$$\frac{1-\phi}{\sqrt{\frac{c_f}{2}}} = Re_f \int_\eta^1 \frac{\frac{\tau}{\tau_w}}{1 + Re_f f_2} d\eta \tag{60}$$

Although $\frac{\tau}{\tau_w}$ and f_2 are taken to be functions of η alone, the indication from (60) is that $\frac{1-\phi}{\sqrt{c_f/2}}$ depends on Re_f as well as on η unless Re_f is large. This result is illustrated by the profiles for Re_f = 25, 100, and 200 in figure 8.

For large Re_f the quantity $(1 + Re_f f_2)$ is approximately equal to $Re_f f_2$ for all $\eta > \eta_1$ except at $\eta = 1$, where $f_2 = 0$. Therefore, for large Re_f (60) becomes

$$\frac{1-\phi}{\sqrt{\frac{c_f}{2}}} = \int_\eta^{1-\Delta} \frac{\frac{\tau}{\tau_w}}{f_2} d\eta + Re_f \int_{1-\Delta}^{1} \frac{\frac{\tau}{\tau_w}}{1 + Re_f f_2} d\eta \tag{61}$$

As indicated by the discussion following equation (48), the last term of (61) becomes negligible for large Re_f. Consequently, for large Re_f (61) becomes

$$\frac{1-\phi}{\sqrt{\frac{c_f}{2}}} = f_1(\eta)$$

or, in the usual form,

$$\frac{u_e - u}{u_\tau} = f_1(\eta) \tag{62}$$

Equation (61) is the velocity defect formula (ref. (1)). Its derivation indicates it to be valid only for sufficiently large Reynolds numbers. The indication from figure 8 is that (62) is valid for the two largest values of Re_f.

The present analysis yields the velocity defect formula and the law of the wall. Explicit expressions for two portions of the law of the wall, namely, the laminar sublayer and the logarithmic portion are obtained. Both the velocity defect and the logarithmic formula require a sufficiently large Reynolds number and, in addition, the logarithmic formula requires that $\frac{\tau}{\tau_w}$ be almost unity.

It is remarked that although $\frac{\epsilon_m}{u_* y}$ is the same function of y_+ for both pipe and plate flow and $\frac{\epsilon_m}{u_* \delta}$ is the same function of η for η less than about .2, the shear ratio is not. The shear distribution in a pipe is

$$\frac{\tau}{\tau_w} = 1 - \frac{y}{r}$$

rather than the distribution shown in figure 1. Consequently, the law of the wall, which was obtained by requiring that $\frac{\tau}{\tau_w}$ be almost unity, should not extend out as far from the wall for pipe flow as for plate flow (see p. 517 of ref. (1)). Moreover, for most of the range of η for which the velocity defect law holds, both $\frac{\epsilon_m}{u_* \delta}$ and $\frac{\tau}{\tau_w}$ are different for pipe than for plate flow. Thus, $\frac{\epsilon_m}{u_* \delta}$ in a pipe remains equal almost to its maximum value out to large values of η instead of dropping to zero. Consequently, the velocity defect formula should be different for pipe than for plate flow (ref. (1)).

Heat-Transfer Coefficient and Temperature Profile

The ratios $\frac{2S_t}{C_f}$ and $\frac{2S_T}{C_F}$ are shown in figure 14. For equal Re_δ, the ratio $\frac{2S_T}{C_F}$ is larger than $\frac{2S_t}{C_f}$ because $\frac{2S_T}{C_F}$ is an average of $\frac{2S_t}{C_f}$ (see eq. (34)) and thus includes the larger values of $\frac{2S_t}{C_f}$ that are present at low values of Re_δ. Also shown in figure 14 is the line

$$\frac{2S_t}{C_f} = \frac{2S_T}{C_F} = Pr^{-\frac{2}{3}}$$

the commonly accepted ratio (p. 497, ref. (2)). The present analysis results in a ratio $\frac{2S_t}{C_f}$ or $\frac{2S_T}{C_F}$ that is larger than $Pr^{-2/3}$ at low Reynolds numbers and smaller at high Reynolds numbers. The behavior at very large Reynolds numbers is obtained from (31). For large Reynolds numbers (31) becomes

$$\frac{1}{S_t Re_\delta Pr} = \frac{1}{Re_f} \int_0^{\frac{52}{Re_f}} \frac{dy_+}{1 + y_+ f_1 Pr} + \int_{\frac{52}{Re_f}}^{1} \frac{\frac{q}{q_w}}{1 + \frac{\epsilon_h}{\epsilon_m} Re_f f_2 Pr} d\eta \qquad (63)$$

or, after taking $\frac{q}{q_w} = 1$ for $\eta < .01$ and $f_2 = K\eta$ for $\frac{52}{Re_f} < \eta < .01$, equation (63) becomes

$$\frac{1}{S_t Re_\delta Pr} = \frac{1}{Re_f}\int_0^{52} \frac{dy_+}{1+y_+ f_1 Pr} + \int_{\frac{52}{Re_f}}^{.01} \frac{d\eta}{1+K\eta Re_f Pr} + \int_{.01}^{1} \frac{\frac{q}{q_w}}{1+\frac{\epsilon_h}{\epsilon_m} Re_f f_2 Pr}\, d\eta \quad (64)$$

For Pr = .738, calculations gave $\frac{15.88}{Re_f}$ for the first integral. The last integral is equal to

$$\frac{1}{Re_f Pr}\int_{.01}^{1-\Delta} \frac{\frac{q}{q_w}}{f_2 \frac{\epsilon_h}{\epsilon_m}}\, d\eta + \int_{1-\Delta}^{1} \frac{\frac{q}{q_w}}{1+\frac{\epsilon_h}{\epsilon_m} Re_f f_2 Pr}\, d\eta$$

which, for large Re_f is equal to $\frac{17.99}{Re_f}$ for Pr = .738. The second integral is integrated analytically. Equation (64) then becomes

$$\frac{1}{S_t Re_\delta} = \frac{Pr}{Re_f}\left[33.87 + \frac{1}{KPr}\ln(1+.01K Re_f Pr) - \frac{1}{KPr}\ln(1+52KPr)\right]$$

or, for .01K Re Pr >> 1,

$$\frac{1}{S_t} = \frac{1}{\sqrt{\frac{C_f}{2}}}\left[2.54 \ln Re_f + 3.04\right]_{(Pr=.738)} \quad (65)$$

When (50) is used for $\sqrt{C_f/2}$, the result is

$$\frac{2S_t}{C_f} = \frac{2.54 \ln Re_f + 6.31}{2.54 \ln Re_f + 3.04} \quad (66)$$

For very large Reynolds numbers (66) becomes

$$\frac{2S_t}{C_f} = 1 \quad (67)$$

The result that the ratio $\frac{2S_t}{C_f}$ approaches unity does not depend on the value of K or of Pr. Because of the logarithm in the numerator and denominator of (66), the ratio approaches unity very slowly. For example, for $Re_f = 10^{10}$, $\frac{2S_t}{C_f} = 1.053$.

From equations (13) and (37) it follows that if $\frac{\epsilon_h}{\epsilon_m} Pr = 1$ for all η, then

$$\frac{t}{\Phi} = \frac{2 S_t Pr}{C_f}$$

or, because $t = \phi = 1$ at $\eta = 1$

$$\frac{2S_t Pr}{C_f} = 1$$

This also follows from (5) and (30). Therefore, the velocity and temperature profiles are identical when $\frac{\epsilon_h}{\nu} \Pr = 1$ for all η. Because $\frac{\epsilon_h}{\epsilon_m}$ depends on η this cannot be so. Consequently, even if $\frac{q}{q_w} = \frac{T}{T_w}$ and $\Pr = 1$ the velocity and temperature profiles are not identical.

For laminar flow, it follows from $\frac{q}{q_w} = \frac{\tau}{\tau_w}$, $\frac{\epsilon_m}{\nu} = 0$, and from (16) and (30) that

$$\frac{2St}{C_f} = \frac{1}{\Pr} \tag{68}$$

The correct result (ref. (2)) is that

$$\frac{2St}{C_f} \cong \Pr^{-\frac{2}{3}} \tag{69}$$

A comparison of equation (16) with equation (30) for $\frac{\epsilon_m}{\nu} = 0$, indicates that the cause of the error is the assumption that $\frac{q}{q_w} = \frac{T}{T_w}$; $\frac{q}{q_w}$ should depend on Pr. Thus, it can be shown from pages 120 and 313 of reference (2) that for laminar flat-plate flow

$$\int_0^\infty \frac{\tau}{\tau_w} d\frac{y}{x}\sqrt{Re_x} = \frac{1}{.332}$$

and that

$$\int_0^\infty \frac{q}{q_w} d\frac{y}{x}\sqrt{Re_x} \cong \frac{1}{.332}\Pr^{-\frac{1}{3}} \tag{70}$$

The quantity $\Pr^{-1/3}$ in (70) accounts for the difference between (68) and (69). The inference is therefore that the effect of Pr on the ratio $\frac{2St}{C_f}$ in the present analysis is inexact. When the Prandtl number is near unity the error is small. Thus, for $\Pr = .738$, the error in (68) is about 12 percent.

Results similar to those obtained for the velocity profiles follow for the temperature profiles. Thus, very close to the wall, $f_1 \ll 1$ and $\frac{q}{q_w} \cong 1$. Equation (38) then becomes

$$t = \frac{S_t \Pr}{\sqrt{\frac{C_f}{2}}} \int_0^{y_+} dy_+ = \frac{S_t \Pr}{\sqrt{\frac{C_f}{2}}} y_+ \tag{71}$$

Define the quantity t* as

$$t_* = -\frac{q_w}{\rho c_p u_*} = \frac{S_t}{\sqrt{\frac{c_f}{2}}}(T_e - T_w)$$ (see ref. (11), p. 823)

Equation (71) then becomes

$$t_+ = Pr\, y_+$$

where

$$t_+ = \frac{T - T_w}{t_*} \qquad (72)$$

This is the linear portion of the temperature profile very close to the wall.

The turbulent shear is equal to the laminar shear where $y_+ f_1$ is equal to unity. This occurs at about $y_+ = 9.9$. From the denominator of the first integral of (38) it follows that the turbulent heat-transfer is equal to the laminar where $y_+ f_1 Pr$ equals unity. For Pr < 1, the so-called edge of the laminar temperature layer is larger than the edge of the laminar velocity layer. Thus, for Pr = .738 the edge of the temperature laminar sublayer is at about $y_+ = 11.4$, a value slightly larger than the value of about 9.9 for the velocity layer.

For y_+ too large for (72) but small enough for $\frac{q}{q_w}$ to be approximately equal to unity, (38) becomes

$$t = \frac{S_t Pr}{\sqrt{\frac{c_f}{2}}} \int_0^{y_+} \frac{dy_+}{f_8(y_+, Pr)}$$

then

$$t_+ = Pr\, f_9(y_+, Pr) \qquad (73)$$

Equation (73) is the law of the wall for the temperature profile. Like the law of the wall for the velocity profile, its upper limit is either the upper limit for f_1 or for $\frac{q}{q_w} \simeq 1$, whichever is smaller.

For the range of η for which (12) is valid, (38) can be written as

$$t = \frac{S_t Pr}{\sqrt{\frac{c_f}{2}}} \int_0^{52} \frac{\frac{q}{q_w}}{1 + y_+ f_1 Pr}\, dy_+ + S_t Re_\delta Pr \int_{\frac{52}{Re_\delta}}^{\eta} \frac{\frac{q}{q_w}}{1 + K\eta Re_\delta \frac{\epsilon_h}{\epsilon_m} Pr}\, d\eta \qquad (74)$$

$$\left(\frac{52}{Re_\delta} \leq \eta \leq .06\right)$$

For large enough Re_δ, $\frac{q}{q_w}$ is almost unity up to values of η large enough to include the upper limit for (12), which is at about .06. Figure 12 indicates that for η between zero and about .06, $\frac{\epsilon_h}{\epsilon_m}$ is almost unity. Therefore, (74) can be written as

$$t = \frac{S_t Pr}{\sqrt{\frac{c_f}{2}}} \int_0^{\delta 2} \frac{dy_+}{1 + y_+ f_1 Pr} + S_t Re_\delta Pr \int_{\frac{\delta 2}{Re_f}}^{\eta} \frac{d\eta}{1 + K\eta Re_f Pr} \qquad (75)$$

$$\left(\frac{\delta 2}{Re_f} \leq \eta \leq .06\right)$$

The first integral in (75) has the value 15.88 for Pr = .738. Equation (75) then becomes

$$t = 11.71 \frac{S_t}{\sqrt{\frac{c_f}{2}}} + \frac{S_t}{K\sqrt{\frac{c_f}{2}}} \ln\left[1 + K\eta Re_f (.738)\right]_{\frac{\delta 2}{Re_f}}^{\eta}$$

or

$$\frac{T - T_w}{t_*} = 11.71 + \frac{1}{K} \ln\left[1 + K\eta Re_f (.738)\right] - \frac{1}{K} \ln\left[1 + \delta 2 K (.738)\right]$$

$$\left(\frac{\delta 2}{Re_f} \leq \eta \leq .06\right)$$

or, with K = .393 and Pr = .738,

$$t_+ = 2.54 \ln \eta + 2.54 \ln Re_f + 1.50 \qquad (76)$$

$$\left(\frac{\delta 2}{Re_f} \leq \eta \leq .06\right)$$

Equation (76) is the logarithmic temperature profile.

A temperature defect formula can be obtained by writing (38) for $\eta = 1$, thus

$$1 = \frac{S_t Pr}{Re_f} \int_0^{y_{+,2}} \frac{\frac{q}{q_w}}{1 + y_+ f_1 Pr} dy_+ + S_t Re_\delta Pr \int_{\eta_2}^{1} \frac{\frac{q}{q_w}}{1 + Re_f f_2 \frac{\epsilon_h}{\epsilon_m} Pr} d\eta \qquad (77)$$

When (38) is subtracted from (77), the result is

$$1 - t = S_t Re_\delta Pr \int_\eta^1 \frac{\frac{q}{q_w}}{1 + Re_f f_2 \frac{\epsilon_h}{\epsilon_m} Pr} d\eta$$

or

$$\frac{(1-t) Re_f}{S_t Re_\delta} = Re_f Pr \int_\eta^1 \frac{\frac{q}{q_w}}{1 + Re_f f_2 \frac{\epsilon_h}{\epsilon_m} Pr} d\eta$$

or, after using the definitions of t, t_*, and Re_f,

$$\frac{Te-T}{t_*} = Re_f Pr \int_{\eta}^{1} \frac{\frac{q}{q_w}}{1 + Re_f f_2 \frac{\epsilon_h}{\epsilon_m} Pr} d\eta \qquad (78)$$

The indication from (78) is that $\frac{Te-T}{t_*}$ depends on Re_f and Pr as well as on η. For large Re_f, however, (78) becomes

$$\frac{Te-T}{t_*} = \int_{\eta}^{1-\Delta} \frac{\frac{q}{q_w}}{f_2 \frac{\epsilon_h}{\epsilon_m}} d\eta + Re_f Pr \int_{1-\Delta}^{1} \frac{\frac{q}{q_w}}{1 + Re_f f_2 \frac{\epsilon_h}{\epsilon_m} Pr} d\eta \qquad (79)$$

where $(1-\Delta)$ is the upper limit of the range of η in which $Re_f f_2 \frac{\epsilon_h}{\epsilon_m} Pr$ is much larger than unity. For very large Re_f, the last term in (79) becomes negligible and (79) becomes

$$\frac{Te-T}{t_*} = f_{10}(\eta) \qquad (80)$$

Equation (80) is a temperature defect profile. The velocity defect profile (eq. (62)) requires only a sufficiently large Re_f. In addition to this requirement, (80) requires that $\frac{q}{q_w}$ and $\frac{\epsilon_h}{\epsilon_m}$ both depend on η alone. Because $\frac{q}{q_w}$ is known to depend on Pr and because $\frac{\epsilon_h}{\epsilon_m}$ probably also does (see p. 552, ref. (1)), equation (80) should more properly be written as

$$\frac{Te-T}{t_*} = f_{11}(\eta, Pr) \qquad (81)$$

Mass-Transfer Coefficient and Concentration Profile

The case treated corresponds to a turbulent boundary layer composed of two species flowing over a plate on which one of the species, say S_1, is condensing or evaporating. The concentration of S_1 is supposed to be so small that the velocity at the wall caused by the evaporation or condensation of S_1 is not large enough to make the concentration profile differ from the shear or heat-transfer profile for $v_w = 0$. If C_1 is the concentration of the evaporating or condensing species, v_w is given by

$$v_w = -\left(\frac{\mathcal{D}}{1-C_1} \frac{\partial C_1}{\partial y}\right)_w \qquad \text{(p. 301 ref. (1))}$$

or

$$\frac{v_w}{u_e} = -\frac{Sc}{Re_\delta} \frac{1}{1-C_{1_w}} \left(\frac{\partial C_1}{\partial \eta}\right)_w$$

All the results obtained for the temperature profiles and heat-transfer coefficients can be converted to the same results for the concentration profiles and mass-transfer coefficients by making the substitutions

$$\delta_t \rightarrow \delta_c$$

$$t \rightarrow \xi$$

$$Pr \rightarrow S_c$$

$$\epsilon_h \rightarrow \epsilon_d$$

$$q \rightarrow m_1$$

$$k \rightarrow \rho D$$

$$T \rightarrow C_1$$

$$T_e \rightarrow C_{1_e}$$

$$T_w \rightarrow C_{1_w}$$

$$S_t \rightarrow C_m$$

and $$C_p \rightarrow 1$$

$$t_* \rightarrow \xi_*$$

where $$\xi_* = \frac{-m_{1w}}{\rho u_*} = \frac{C_m}{\sqrt{\frac{C_f}{2}}}\left(C_{1e} - C_{1w}\right)$$

CONCLUDING REMARKS

It has been shown that the friction coefficient for a constant property, zero pressure gradient, turbulent boundary layer can be calculated over the entire range of Reynolds numbers by one method. The method is to use the relation between the local shear, the local sum of the molecular and eddy viscosity, and the local velocity gradient. The eddy viscosity across the boundary layer is obtained by joining a distribution for the wall region to one for the outer region. The same procedure yields the velocity profile from the wall to the outer edge of the boundary layer without using the concept of laminar sublayer, transition region, logarithmic region, etc.

The heat and mass-transfer coefficient and the temperature and concentration profile are calculated by a similar method. More approximations, however, are used than to calculate the friction coefficient and velocity profile. Therefore, these results are probably not as accurate as those for the velocity

boundary layer. For example, although the calculated friction coefficient, $C_f/2$, agrees closely with accepted values, the ratio $\frac{2St}{C_f}$ differs slightly from the accepted value, $Pr^{-2/3}$, and decreases with increasing Reynolds number.

REFERENCES

(1) Hinze, J. O., "Turbulence," McGraw-Hill Book Co., Inc., 1959

(2) Schlichting, H., "Boundary-Layer Theory," McGraw-Hill Book Co., Inc., 1960

(3) Hanratty, T. J., and Johnk, R. E., "Development of Temperature Profile for Turbulent Heat Exchange in a Pipe," Tech. Rept. No. 10, University of Illinois, Urbana, 1961

(4) Fediaevsky, K., "Turbulent Boundary-Layer of an Airfoil," NACA TM 822, 1937, also JAS, Vol. 4, No. 12, Oct. 1937

(5) Klebanoff, P. S., "Characteristics of Turbulence in a Boundary Layer with Zero Pressure Gradient," NACA TR 1247, 1955

(6) Cavers, S. D., Hsu, N. T., Schlinger, W. G., and Sage, B. H., "Temperature Gradients in Turbulent Gas Streams," Industrial and Engineering Chemistry, Vol. 45, No. 10, Oct. 1953

(7) Page, F. Jr., Schlinger, W. G., Breaux, D. K., Sage. B. H., "Point Values of Eddy Conductivity and Viscosity In Uniform Flow Between Parallel Plates," Industrial and Engineering Chemistry, Vol. 44, No. 2, February 1952

(8) Lin, C. C. (ed.), "Turbulent Flows and Heat Transfer," Vol. V, High-Speed Aerodynamics and Jet Propulsion, Princeton University Press, 1959, Princeton, New Jersey

(9) Preston, J. H., "The Minimum Reynolds Number for a Turbulent Boundary Layer and the Selection of a Transition Device," Jour. of Fluid Mech., Vol. 3, Part 4, pp. 373-384, Jan. 1958

(10) Landweber, L., "The Frictional Resistance of Flat Plates in Zero Pressure Gradient," Trans. Soc. Nav. Archit. New York 61, 5, 1953

(11) Howarth, L. (ed.), "Modern Developments in Fluid Dynamics, High-Speed Flow," Vol. II, Oxford, 1953

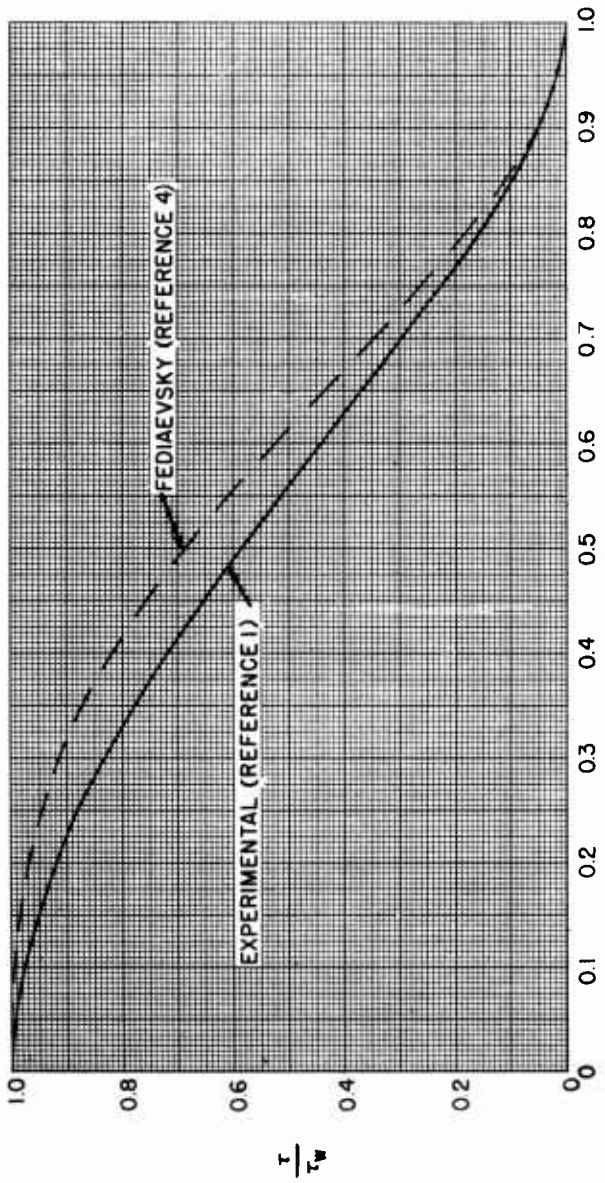

FIG. 1 RATIO OF LOCAL TO WALL SHEAR AS A FUNCTION OF RATIO OF WALL DISTANCE TO BOUNDARY LAYER THICKNESS

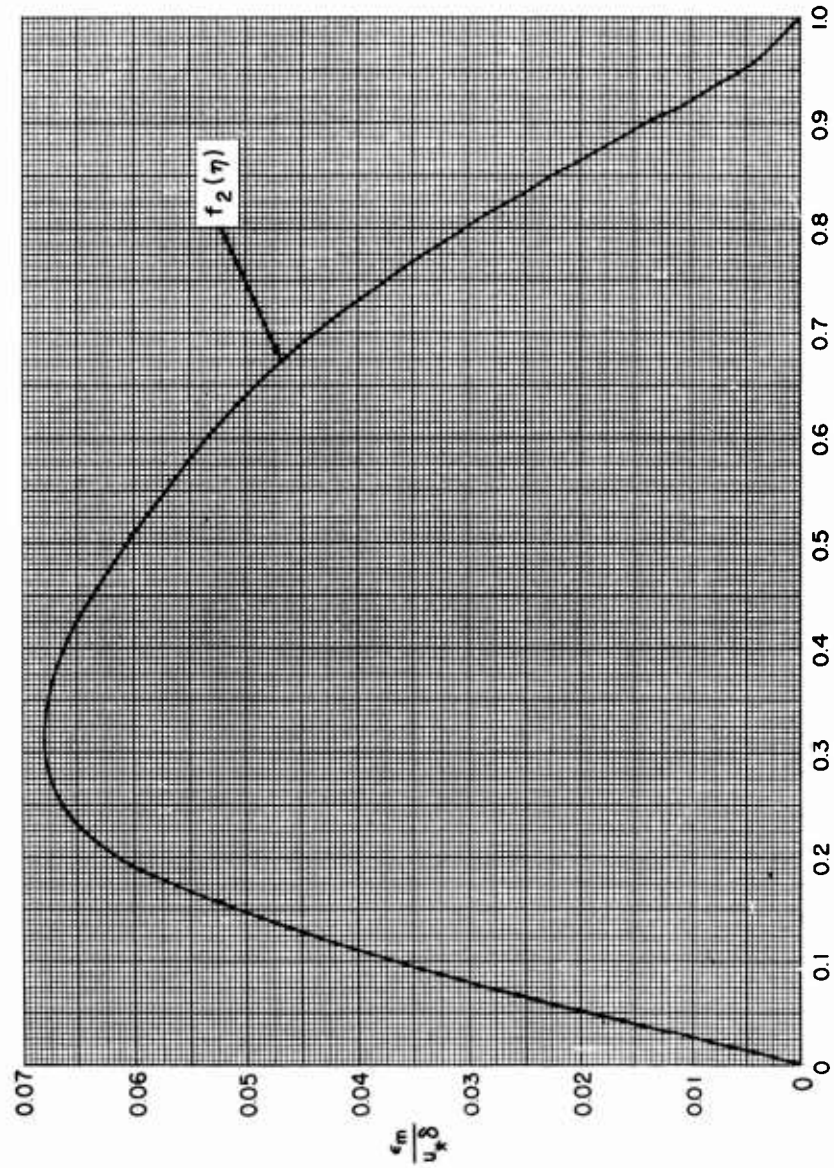

FIG. 2 RECIPROCAL OF EDDY KINEMATIC VISCOSITY REYNOLDS NUMBER AS A FUNCTION OF RATIO OF WALL DISTANCE TO BOUNDARY LAYER THICKNESS

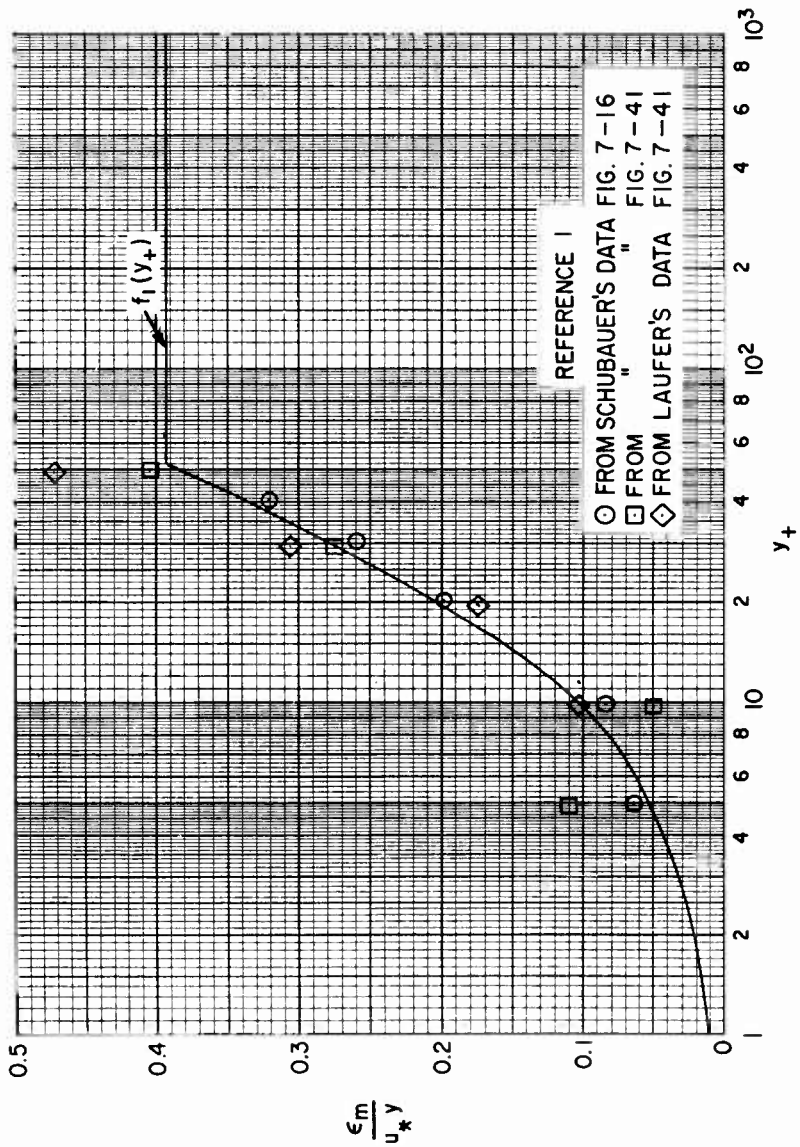

FIG. 3 RECIPROCAL OF EDDY KINEMATIC VISCOSITY WALL DISTANCE REYNOLDS NUMBER AS A FUNCTION OF THE KINEMATIC VISCOSITY WALL DISTANCE REYNOLDS NUMBER

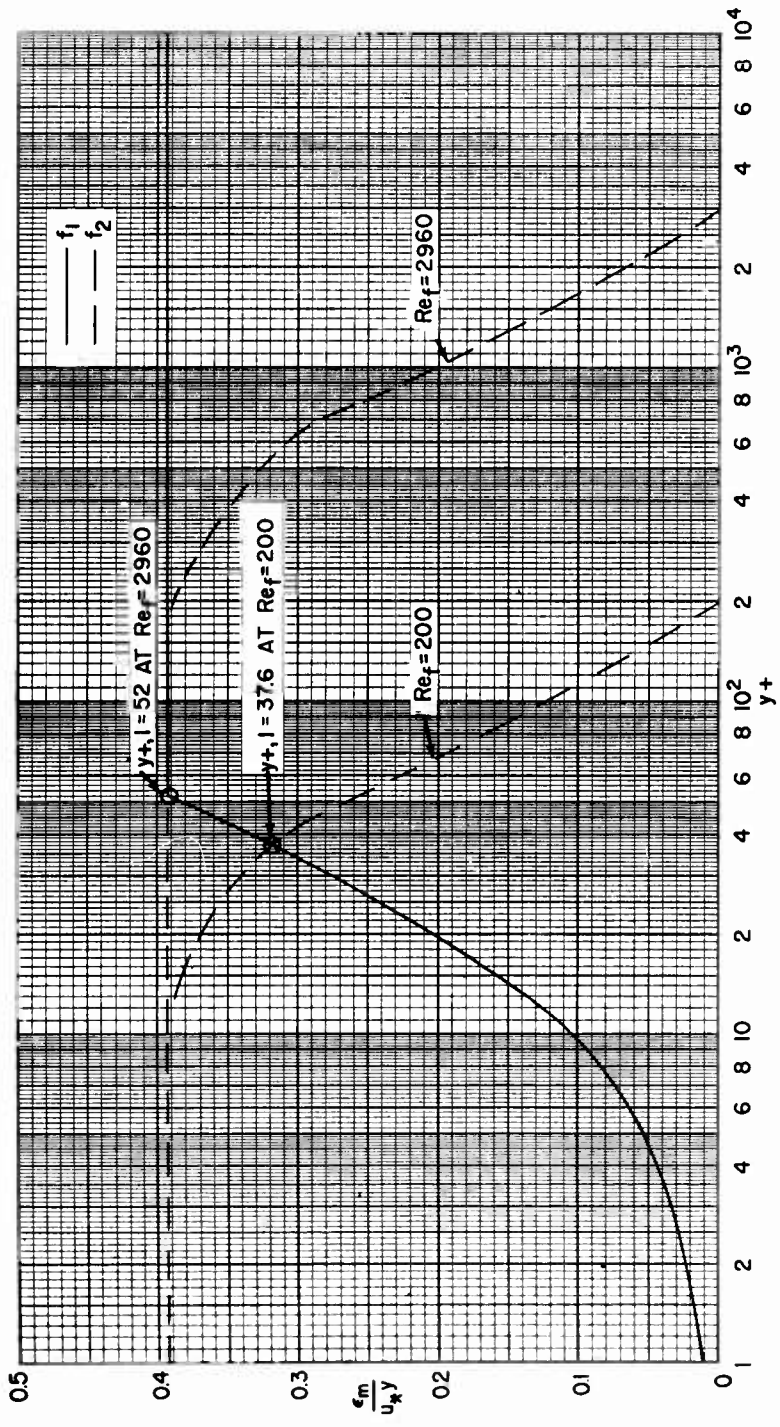

FIG. 4 DETERMINATION OF $y+,1$ AT $Re_f = 200$ AND AT $Re_f = 2960$

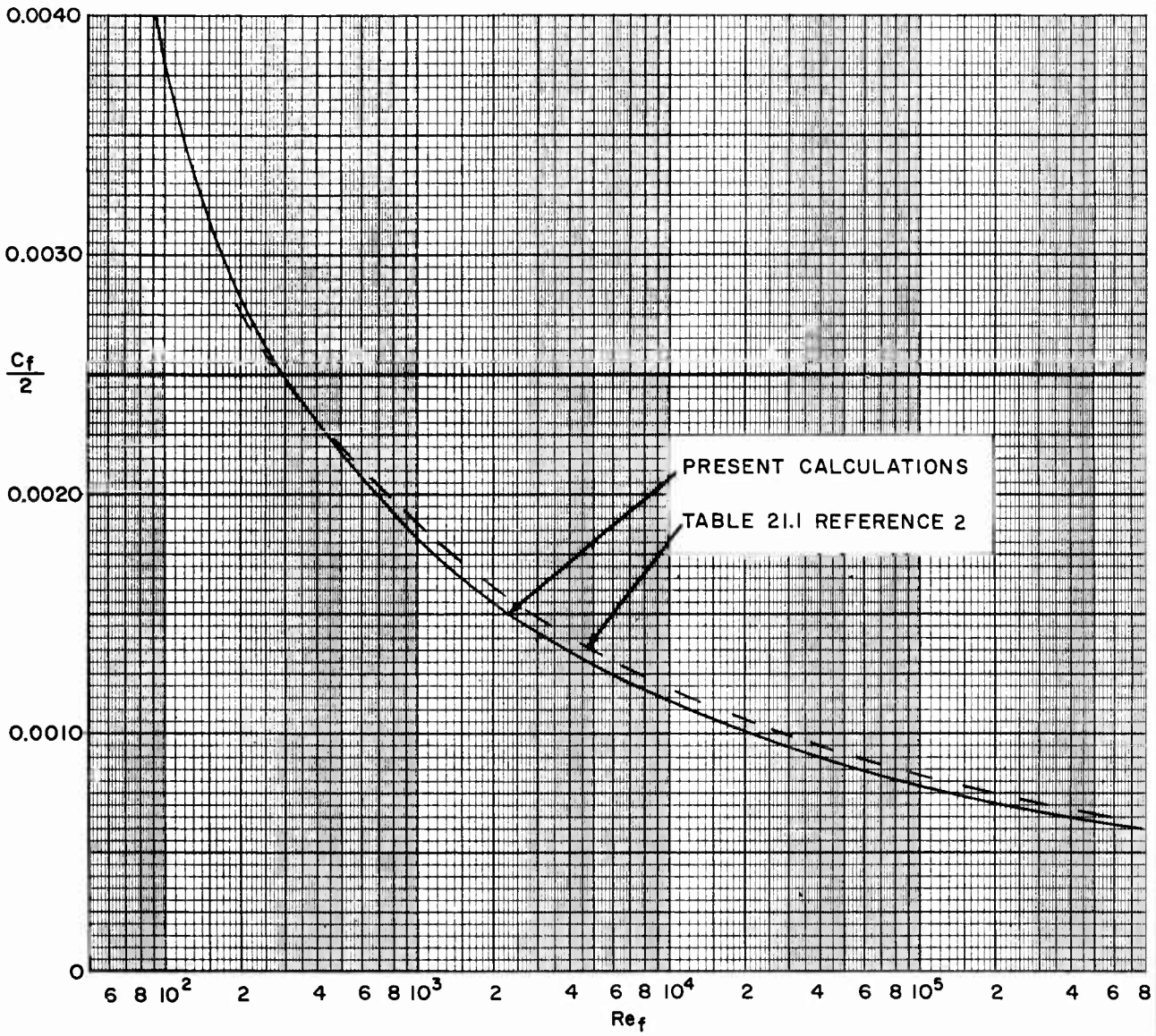

FIG.5 LOCAL FRICTION COEFFICIENT AS A FUNCTION OF BOUNDARY LAYER FRICTION REYNOLDS NUMBER

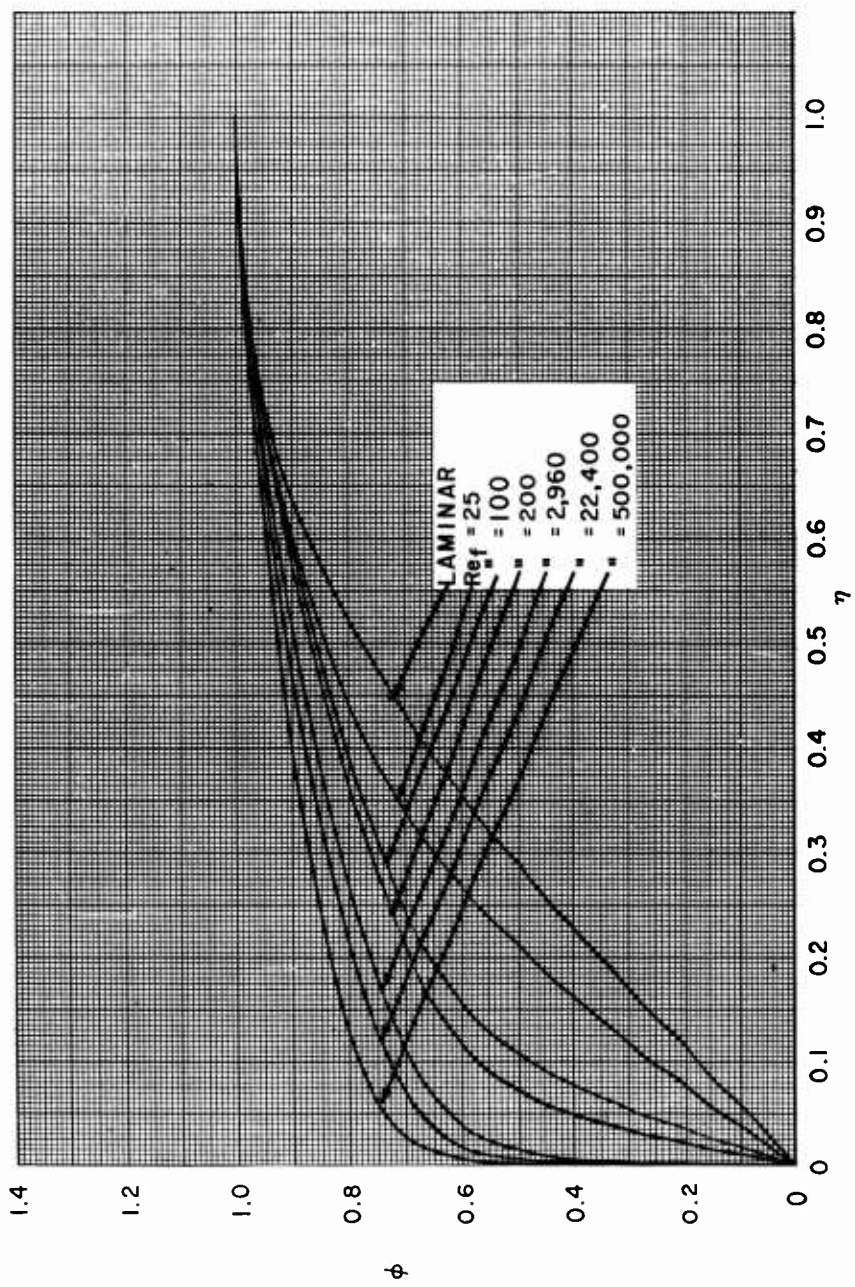

FIG. 6 NON-DIMENSIONAL VELOCITY PROFILES FOR SIX FRICTION REYNOLDS NUMBERS

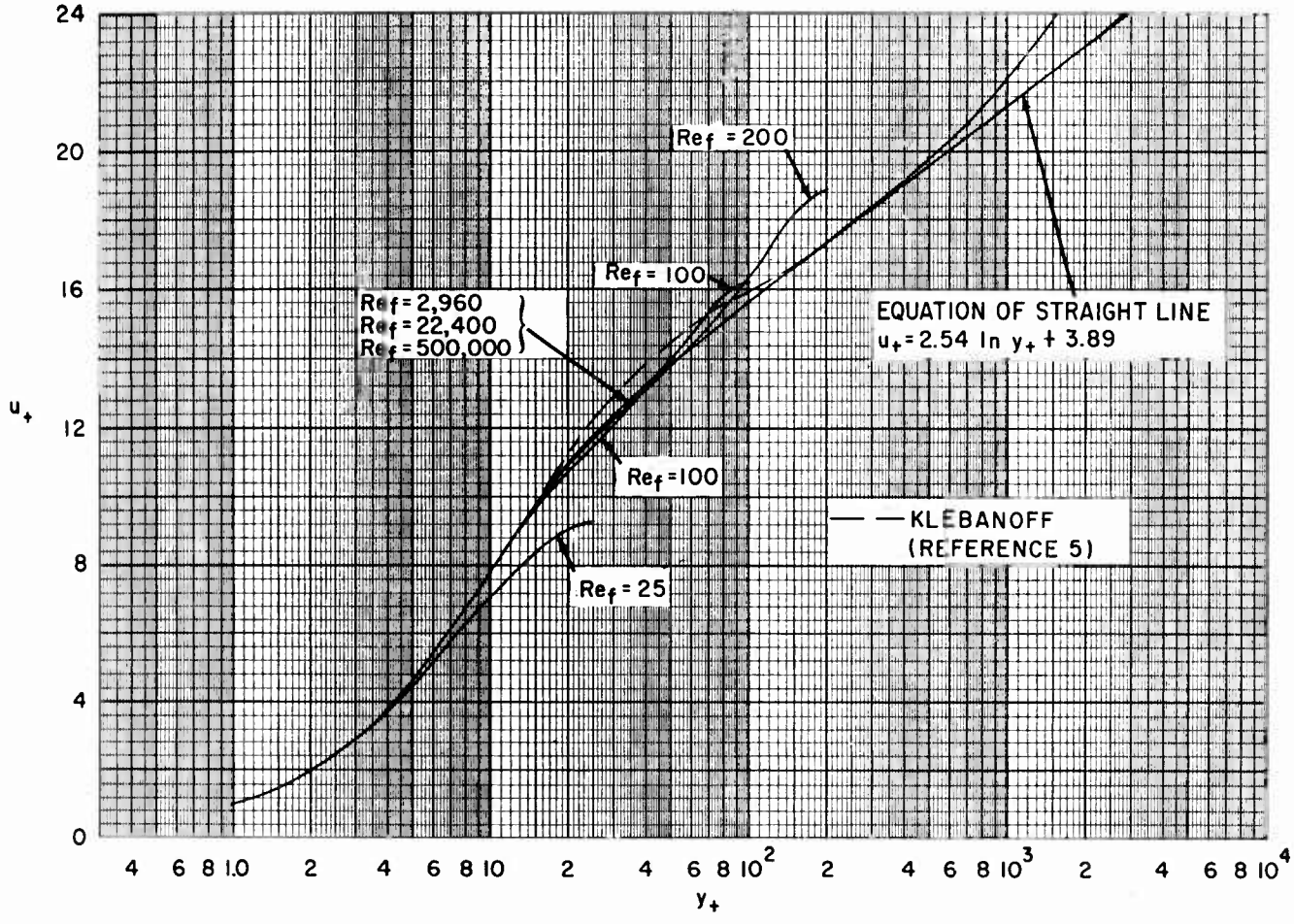

FIG. 7A RATIO OF LOCAL VELOCITY TO FRICTION VELOCITY AS A FUNCTION OF WALL DISTANCE REYNOLDS NUMBER FOR SIX FRICTION REYNOLDS NUMBERS

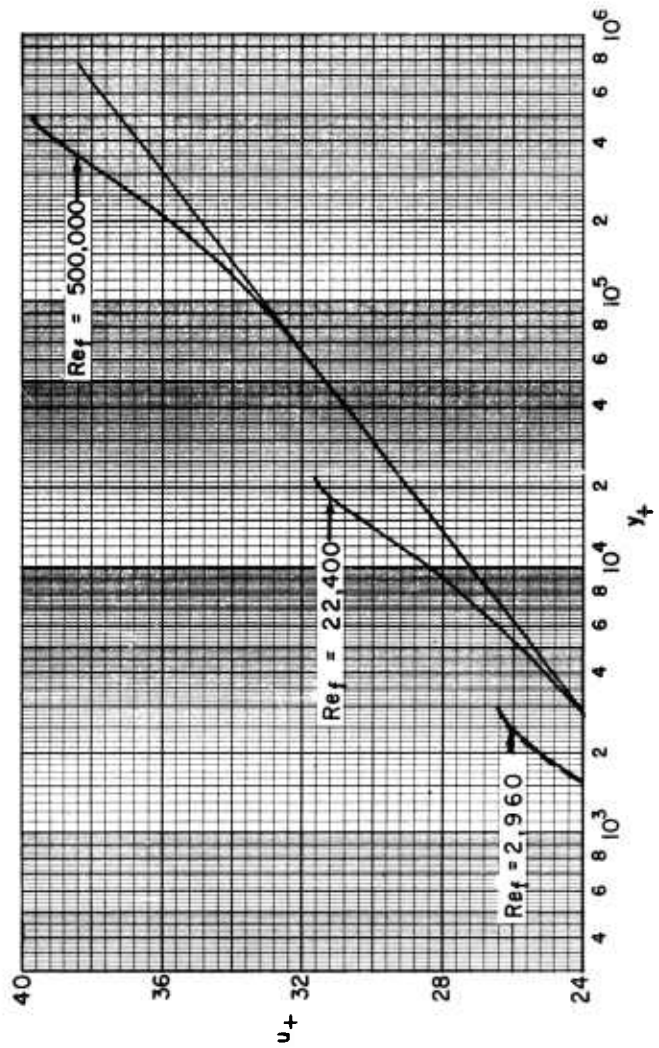
Ref = 500,000
Ref = 22,400
Ref = 2,960
40
36
32
28
24
u+
4 6 8 10^3 2 4 6 8 10^4 2 4 6 8 10^5 2 4 6 8 10^6
y+

FIG.78

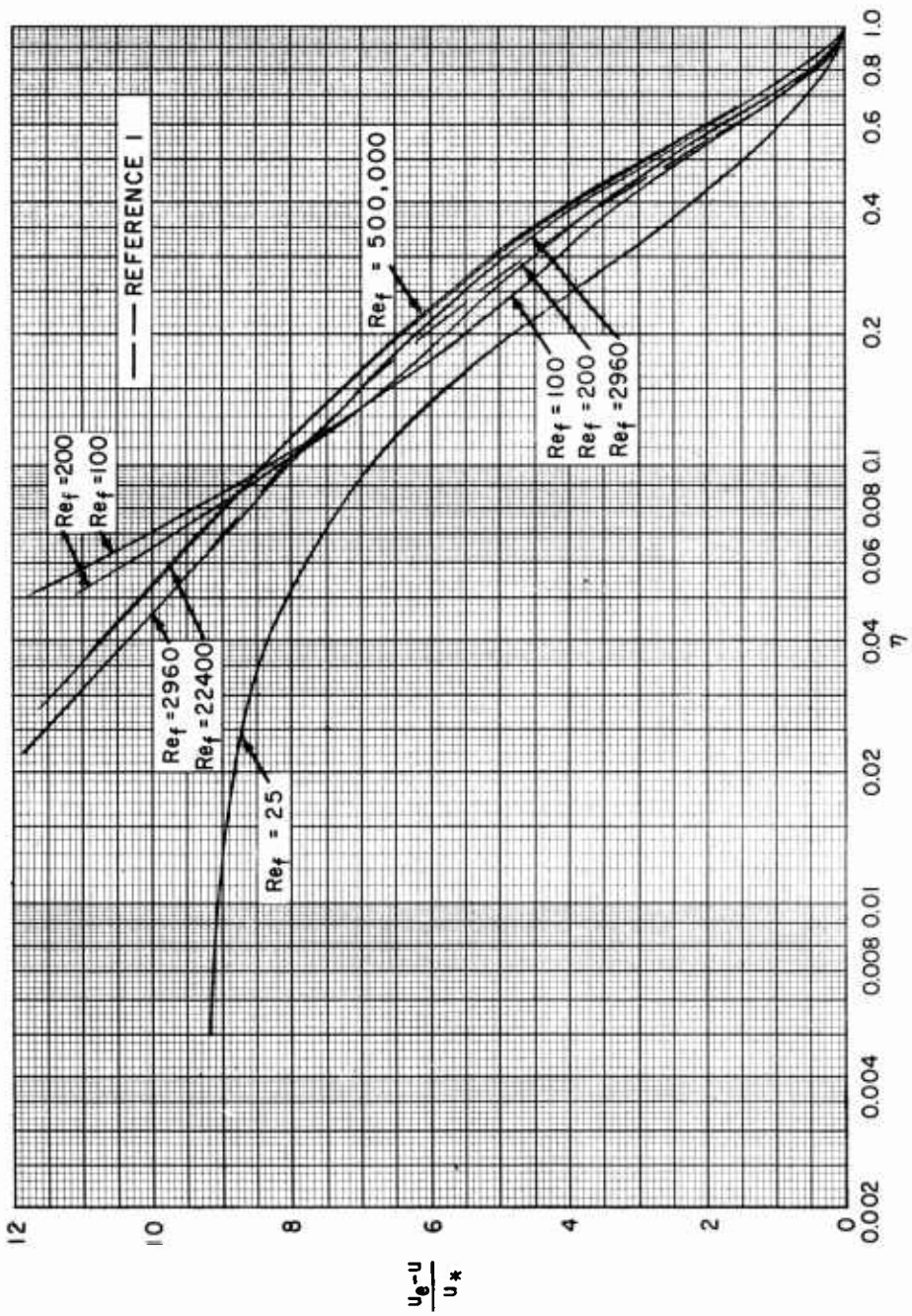

FIG. 8 VELOCITY DEFECT AS A FUNCTION OF RATIO OF WALL DISTANCE TO BOUNDARY-LAYER THICKNESS FOR SIX FRICTION REYNOLDS NUMBERS

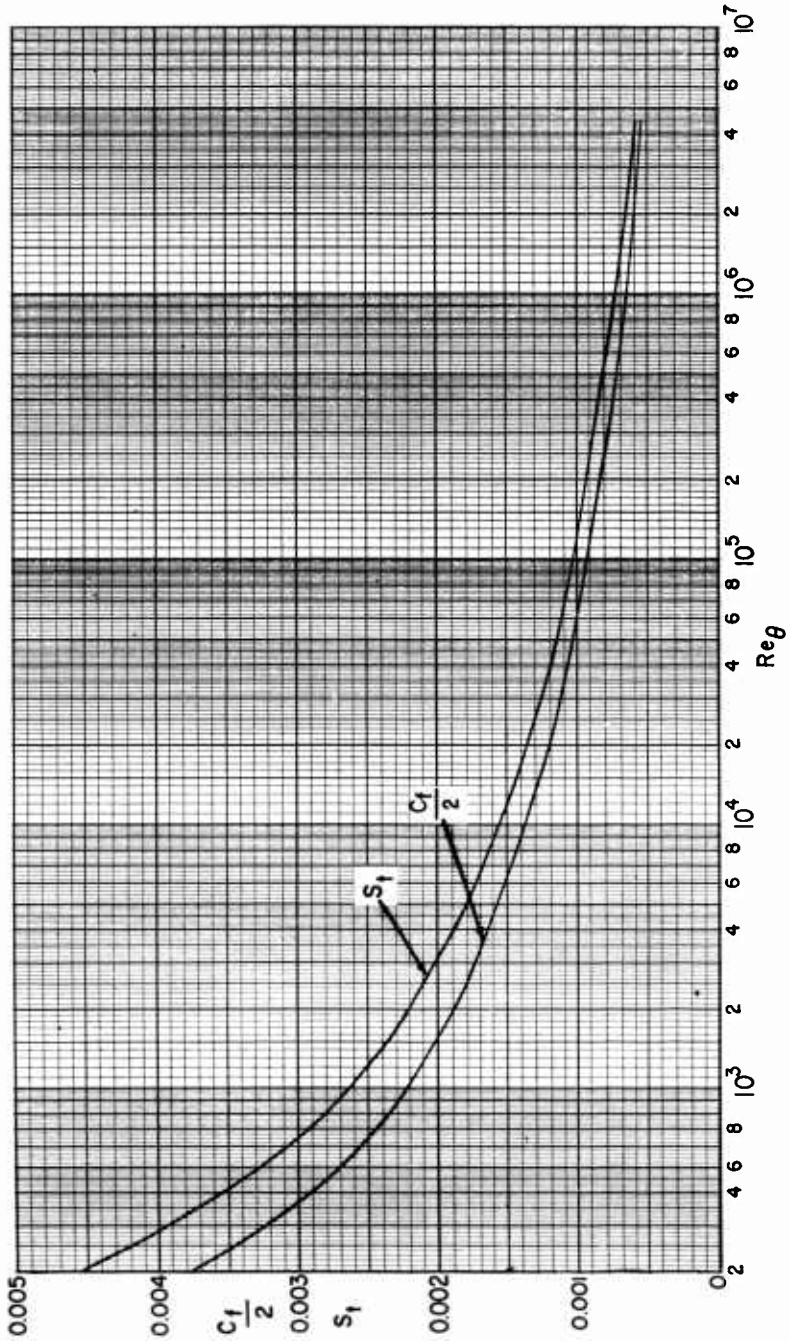

FIG. 9 LOCAL FRICTION COEFFICIENT AND LOCAL STANTON NUMBER AS A FUNCTION OF BOUNDARY LAYER MOMENTUM THICKNESS REYNOLDS NUMBER

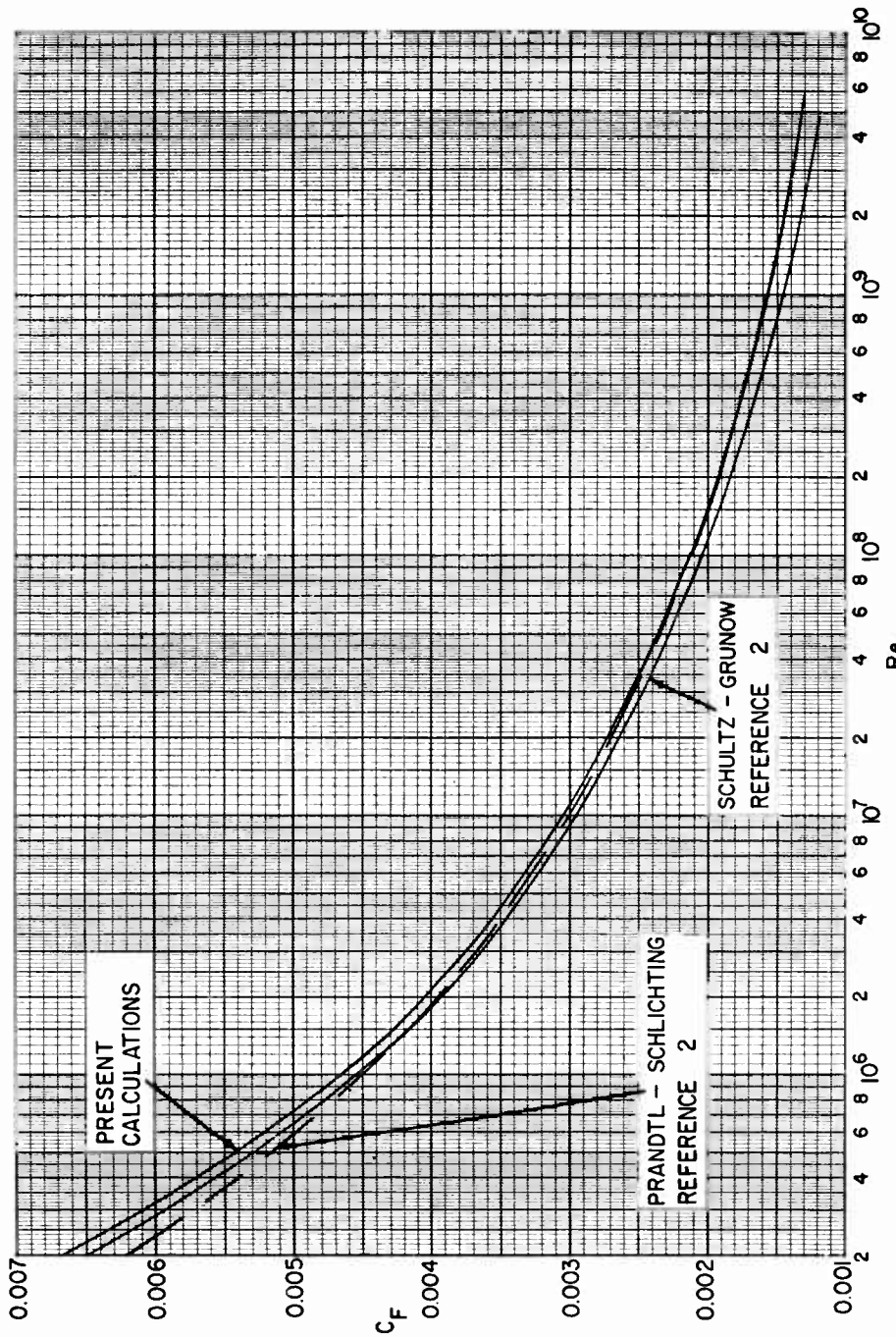

FIG. 10 AVERAGE FRICTION COEFFICIENT AS A FUNCTION OF REYNOLDS NUMBER BASED ON DISTANCE TO LEADING EDGE

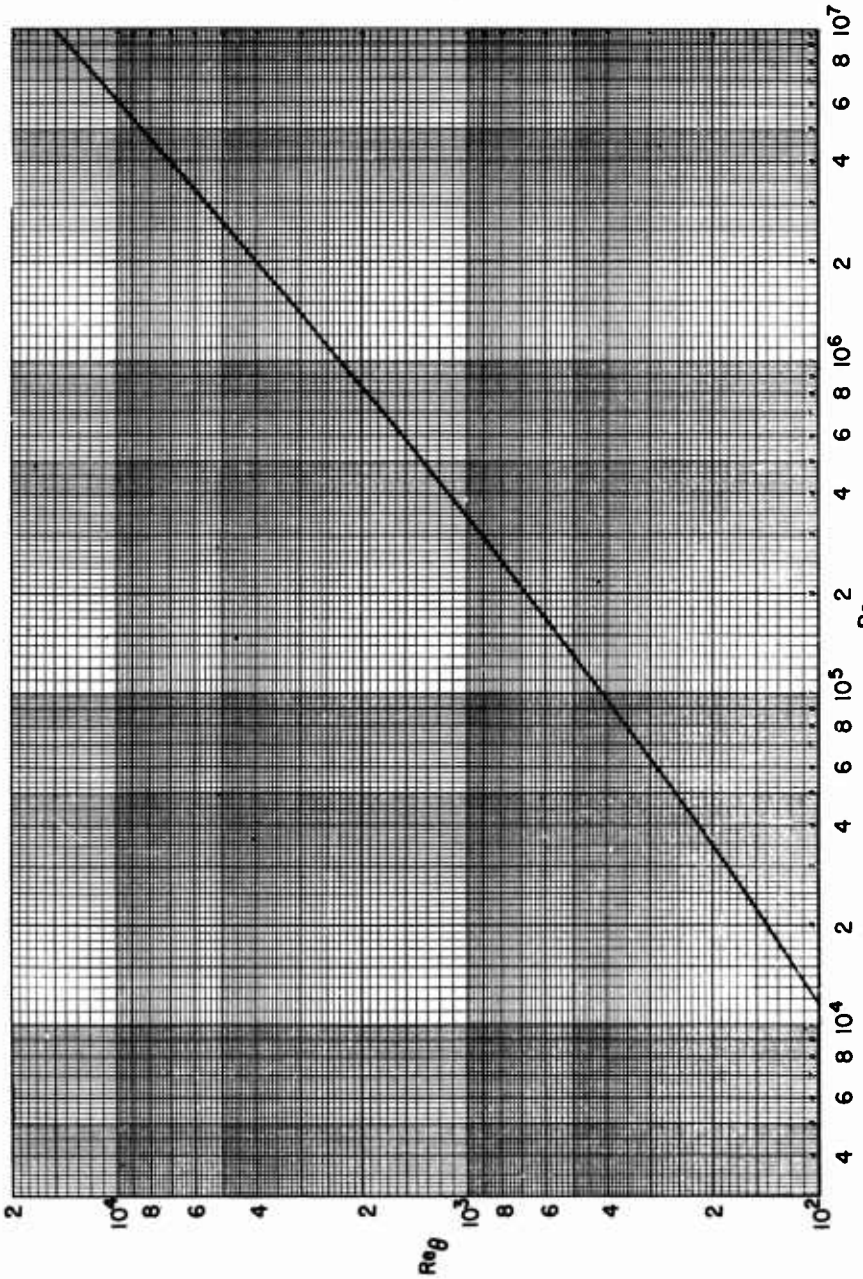

FIG. 11A BOUNDARY LAYER MOMENTUM THICKNESS REYNOLDS NUMBER AS A FUNCTION OF REYNOLDS NUMBER BASED ON DISTANCE TO LEADING EDGE

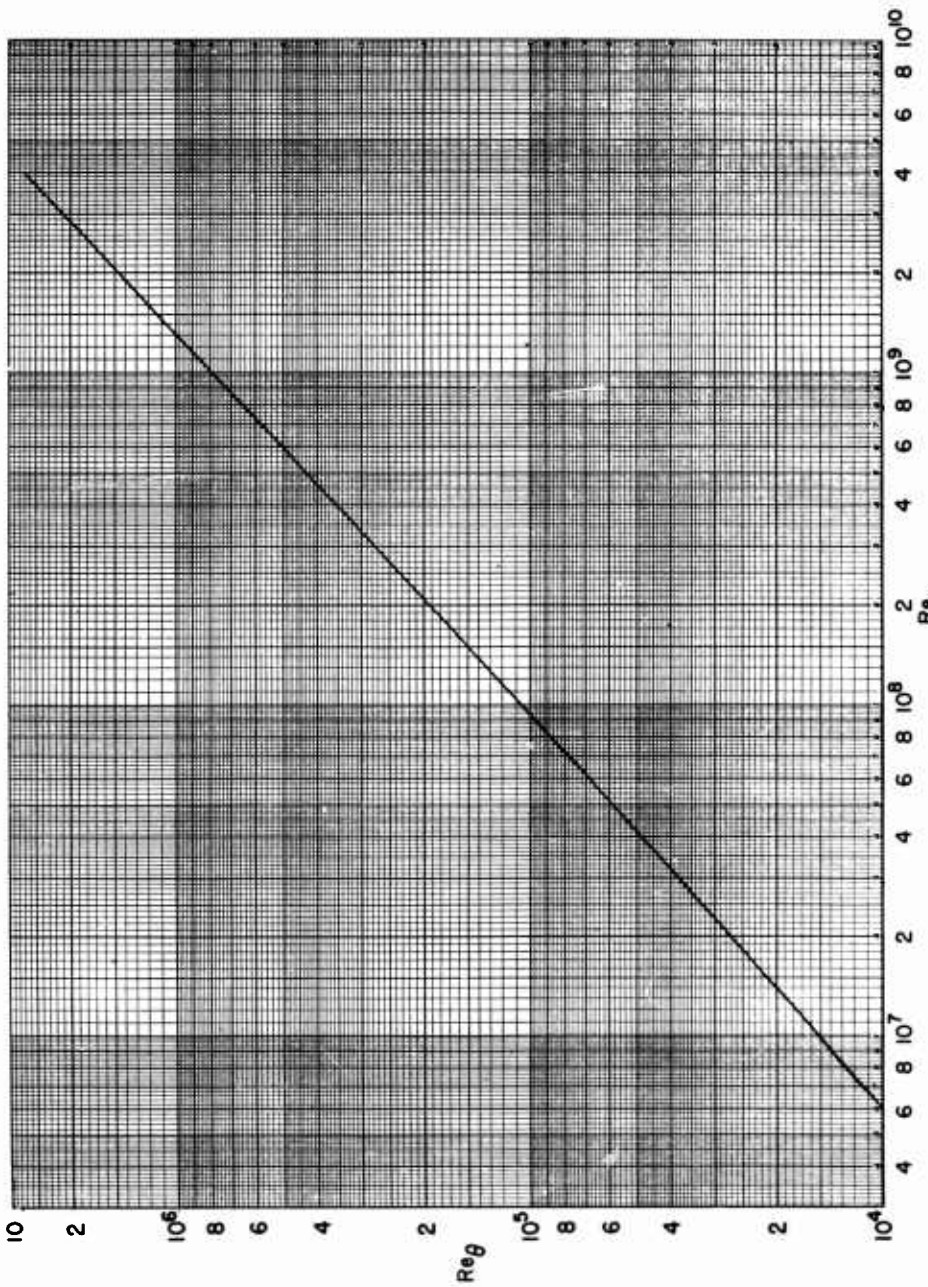
10
2
10^6
8
6
4
2
10^5
8
6
4
2
10^4
Re_θ
4
6
8
10^7
2
4
6
8
10^8
2
Re_x
4
6
8
10^9
2
4
6
8
10^{10}

FIG. 11B

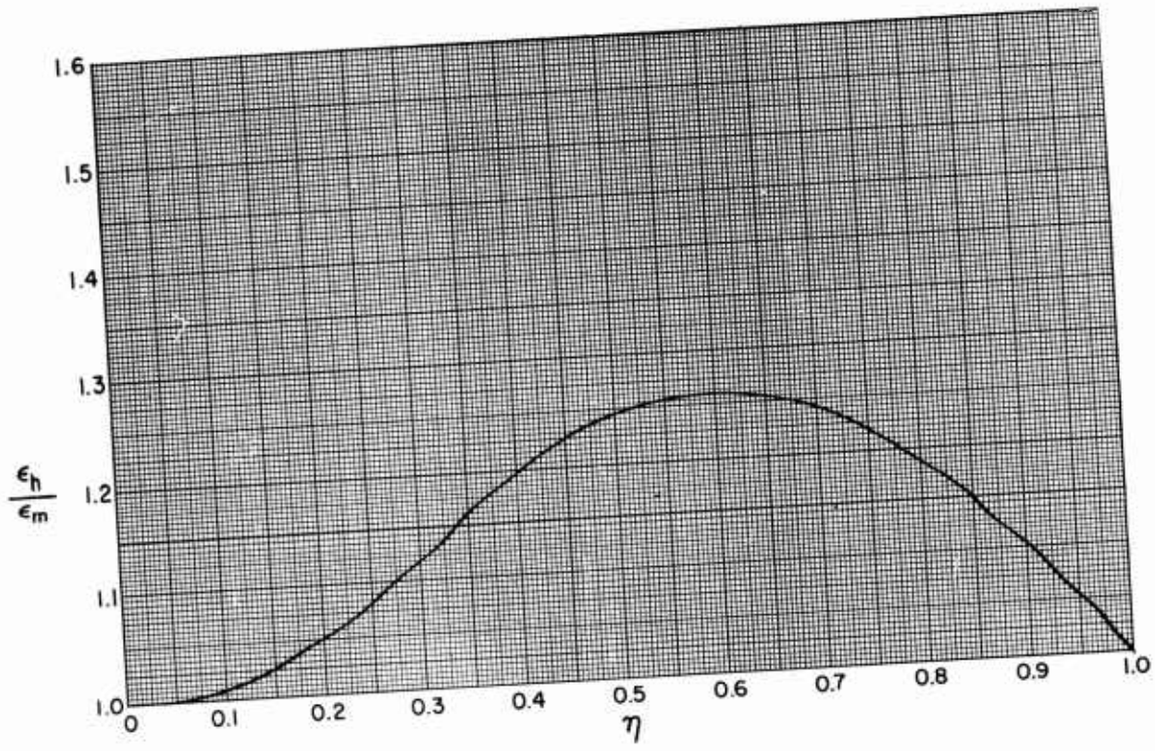

FIG. 12 RATIO OF EDDY THERMAL DIFFUSIVITY TO EDDY KINEMATIC VISCOSITY AS A FUNCTION OF RATIO OF WALL DISTANCE TO BOUNDARY LAYER THICKNESS

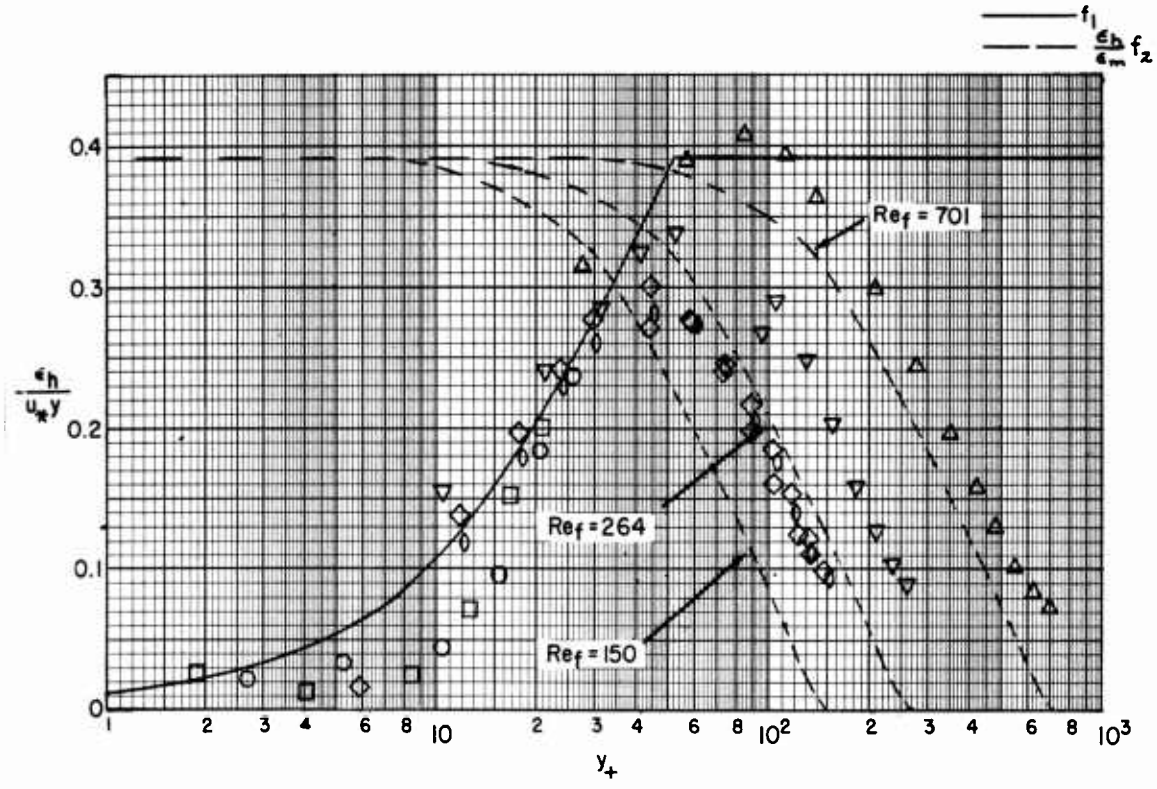

FIG. 13 EXPERIMENTAL VARIATION OF $\frac{\epsilon_h}{u_* y}$ WITH y_+ FOR A CHANNEL AND CALCULATED VARIATION FOR A PLATE

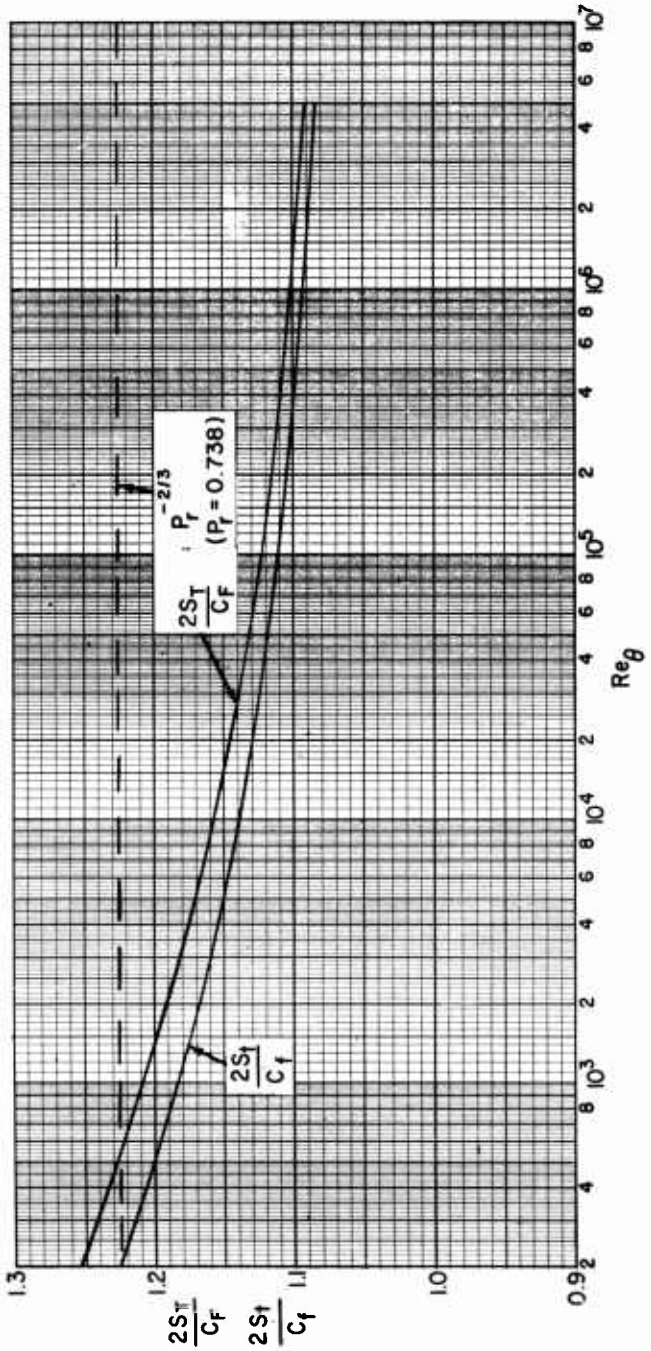

FIG. 14 RATIO OF LOCAL AND AVERAGE STANTON NUMBER TO LOCAL AND AVERAGE FRICTION COEFFICIENT, RESPECTIVELY, AS A FUNCTION OF BOUNDARY LAYER MOMENTUM THICKNESS REYNOLDS NUMBER.

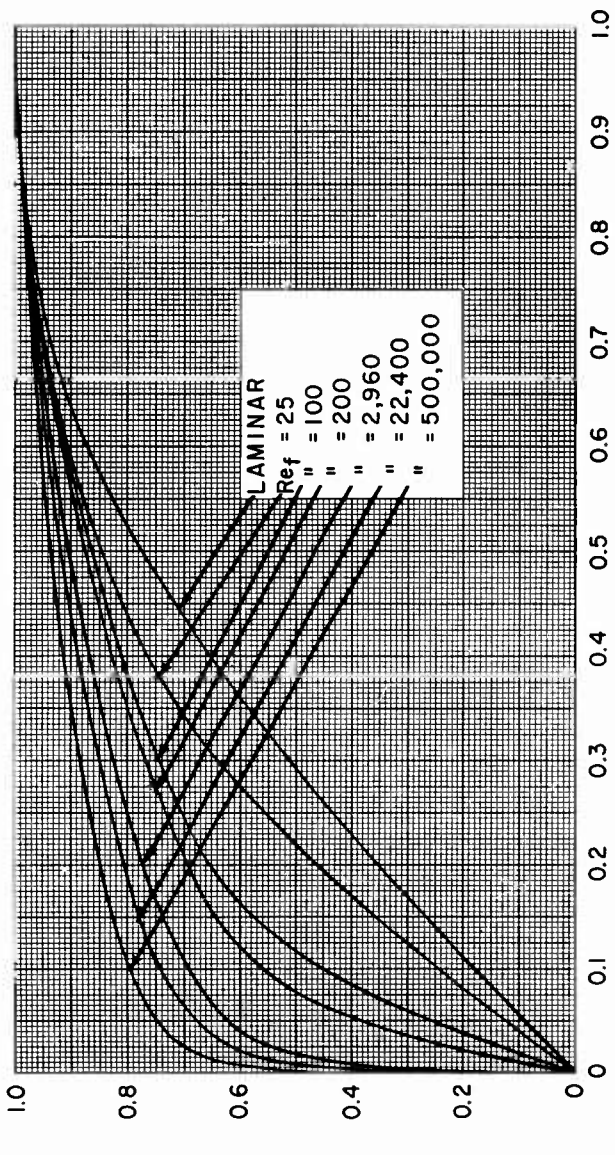

FIG.15 NON-DIMENSIONAL TEMPERATURE PROFILES FOR SIX FRICTION REYNOLDS NUMBERS

TABLE I

Limit of Wall Region and Associated Eddy Kinematic Viscosity Reynolds Number For Three Friction Reynolds Numbers

Re_f	$\left(\frac{\epsilon_m}{u_* y}\right)_1$	$y_{+,1}$	$\left(\frac{\epsilon_m}{u_* \delta}\right)_1$	η_1
25	.127	12.2	.0615	.487
100	.253	26.6	.0672	.266
200	.318	37.6	.0598	.188

TABLE II

Friction Coefficient and Boundary Layer Reynolds Number for Six Friction Reynolds Numbers

Re_f	$C_f/2$	Re_δ
25	.0116	2.32×10^2
100	.00378	1.62×10^3
200	.00280	3.78×10^3
2,960	.00143	7.81×10^4
22,400	.000987	7.13×10^5
500,000	.000633	1.99×10^7

TABLE III

Calculated Velocity Profiles

Re_f = 25		Re_f = 100		Re_f = 200		Re_f = 2960		Re_f = 22,400		Re_f = 5×10^5		Laminar	
η	ϕ	η	ϕ	η	ϕ	η	ϕ	η	ϕ	η	ϕ	η	ϕ
.04	.107	.01	.061	.005	.053	.00068	.074	.005	.500	.0025	.552	.01	.018
.08	.211	.02	.121	.01	.103	.00135	.143	.01	.554	.005	.596	.05	.091
.12	.309	.03	.179	.02	.199	.00202	.203	.02	.609	.01	.640	.10	.181
.16	.400	.04	.233	.04	.353	.00338	.294	.03	.641	.02	.634	.20	.355
.20	.483	.06	.330	.05	.411	.00676	.412	.04	.664	.04	.729	.30	.516
.24	.553	.10	.477	.10	.575	.0101	.467	.05	.681	.06	.755	.40	.658
.32	.675	.15	.595	.15	.649	.0176	.528	.06	.694	.16	.821	.50	.777
.40	.765	.20	.662	.175	.673	.0203	.541	.16	.776	.26	.858	.60	.871
.487	.834	.25	.708	.188	.683	.0270	.568	.36	.862	.36	.888	.70	.938
.51	.848	.266	.720	.21	.700	.0676	.654	.56	.926	.46	.916	.80	.979
.61	.904	.36	.781	.41	.821	.169	.746	.76	.972	.56	.940	.90	.997
.71	.947	.46	.838	.61	.913	.236	.784	.96	.998	.66	.960	1.00	1.000
.81	.976	.56	.888	.81	.976	.372	.848	1.00	1.000	.76	.976		
.91	.992	.66	.930	.91	.993	.574	.920			.86	.989		
1.00	1.000	.76	.963	1.00	1.000	.777	.974			.96	.999		
		.86	.986			1.000	1.000			1.00	1.000		
		.96	.997										
		1.00	1.000										

TABLE IV

Computed Values of $\frac{\theta}{\delta}$, $\frac{\delta^*}{\delta}$, and $\frac{\delta^*}{\theta}$ for Six Friction Reynolds Numbers

Re_f	$\frac{\theta}{\delta}$	$\frac{\delta^*}{\delta}$	$\frac{\delta^*}{\theta}$	$Re_\theta \times 10^{-3}$
25	.119	.269	2.25	.0277
100	.118	.211	1.79	.191
200	.117	.189	1.61	.444
2,960	.102	.138	1.35	7.98
22,400	.0922	.119	1.29	65.7
500,000	.0791	.0954	1.21	1571.

TABLE V

Limit of Wall Region and Associated Eddy Thermal Diffusivity Reynolds Number for Three Friction Reynolds Numbers

Re_τ	$\left(\frac{\epsilon_h}{u_* y}\right)$	$y_{+,2}$	$\left(\frac{\epsilon_m}{u_* \delta}\right)\left(\frac{\epsilon_h}{\epsilon_m}\right)$	η_2
25	.140	13.2	.0736	.528
100	.266	28.4	.0750	.284
200	.328	39.0	.0639	.195

TABLE VI

Local Stanton Number, Ratio of Stanton Number to Friction Coefficient, and Boundary-Layer Momentum Thickness Reynolds Number for Six Friction Reynolds Numbers

Re_f	S_t	$\frac{2S_t}{C_f}$	$Re_\theta \times 10^{-3}$
25	.0148	1.28	.0277
100	.00463	1.22	.191
200	.00339	1.21	.444
2,960	.00164	1.14	7.98
22,400	.00110	1.12	65.7
500,000	.00069	1.09	1571.

TABLE VII

Calculated Temperature Profiles

Re_x = 25		Re_f = 100		Re_f = 200		Re_f = 2960		Re_f = 22,400		Re_f = $5x10^5$		Laminar	
η	t	η	t	η	t	η	t	η	t	η	t	η	t
.04	.101	.01	.055	.005	.047	.00068	.063	.00232	.413	.01	.636	.01	.018
.08	.200	.02	.110	.01	.094	.00135	.122	.01	.539	.02	.684	.05	.091
.12	.294	.03	.163	.02	.182	.00202	.176	.02	.600	.04	.733	.10	.181
.16	.383	.04	.213	.04	.328	.00338	.262	.06	.697	.06	.761	.20	.355
.20	.465	.06	.306	.05	.384	.00676	.384	.16	.788	.16	.832	.30	.516
.24	.540	.10	.454	.10	.561	.0101	.443	.36	.875	.26	.870	.40	.658
.32	.667	.15	.580	.15	.645	.0176	.508	.56	.933	.36	.900	.50	.777
.40	.764	.20	.656	.175	.673	.0203	.524	.76	.974	.46	.924	.60	.871
.48	.835	.25	.708	.195	.691	.0270	.554	.96	.999	.56	.945	.70	.938
.528	.868	.284	.736	.21	.703	.0676	.651	1.00	1.000	.66	.963	.80	.979
.56	.887	.31	.754	.41	.830	.169	.755			.76	.978	.90	.997
.61	.912	.41	.817	.61	.920	.236	.796			.86	.989	1.00	1.000
.71	.955	.51	.870	.81	.980	.372	.859			.96	.998		
.81	.984	.61	.914	.91	.998	.574	.926			1.00	1.000		
.91	.999	.71	.950	1.00	1.000	.777	.975						
1.00	1.000	.81	.978			1.000	1.000						
		.91	.995										
		.96	.999										
		1.00	1.000										

AERODYNAMICS DEPARTMENT
EXTERNAL DISTRIBUTION LIST (A1)

	No. of Copies
Chief, Bureau of Naval Weapons Department of the Navy Washington 25, D. C.	
Attn: DLI-30	1
Attn: R-14	1
Attn: RRRE-4	1
Attn: RMGA-413	1
Office of Naval Research Room 2709, T-3 Washington 25, D. C.	
Attn: Head, Mechanics Branch	1
Director, David Taylor Model Basin Aerodynamics Laboratory Washington 7, D. C.	
Attn: Library	1
Commander, U. S. Naval Ordnance Test Station China Lake, California	
Attn: Technical Library	1
Attn: Code 503	1
Attn: Code 406	1
Director, Naval Research Laboratory Washington 25, D. C.	
Attn: Code 2027	1
Commanding Officer Office of Naval Research Branch Office Box 39, Navy 100 Fleet Post Office New York, New York	1
NASA High Speed Flight Station Box 273 Edwards Air Force Base, California	
Attn: W. C. Williams	1
NASA Ames Research Center Moffett Field, California	
Attn: Librarian	1

AERODYNAMICS DEPARTMENT
EXTERNAL DISTRIBUTION LIST (A1)

	No. of Copies
NASA Langley Research Center Langley Field, Virginia	
Attn: Librarian	3
Attn: C. H. McLellan	1
Attn: J. J. Stack	1
Attn: Adolf Busemann	1
Attn: Comp. Res. Div.	1
Attn: Theoretical Aerodynamics Division	1
NASA Lewis Research Center 21000 Brookpark Road Cleveland 11, Ohio	
Attn: Librarian	1
Attn: Chief, Propulsion Aerodynamics Div.	1
NASA 1520 H Street, N. W. Washington 25, D. C.	
Attn: Chief, Division of Research Information	1
Attn: Dr. H. H. Kurzweg, Asst. Director of Research	1
Office of the Assistant Secretary of Defense (R&D) Room 3E1065, The Pentagon Washington 25, D. C.	
Attn: Technical Library	1
Research and Development Board Room 3D1041, The Pentagon Washington 25, D. C.	
Attn: Library	1
ASTIA Arlington Hall Station Arlington 12, Virginia	10
Commander, Pacific Missile Range Point Mugu, California	
Attn: Technical Library	1
Commanding General Aberdeen Proving Ground, Maryland	
Attn: Technical Information Branch	1
Attn: Ballistic Research Laboratory	1

AERODYNAMICS DEPARTMENT
EXTERNAL DISTRIBUTION LIST (A1)

	No. of Copies
Commander, Naval Weapons Laboratory Dahlgren, Virginia Attn: Library	1
Director, Special Projects Department of the Navy Washington 25, D. C. Attn: SP-2722	1
Director of Intelligence Headquarters, USAF Washington 25, D. C. Attn: AFOIN-3B	1
Headquarters - Aero. Systems Division Wright-Patterson Air Force Base Dayton, Ohio Attn: WWAD Attn: RRLA-Library	2 1
Commander Air Force Ballistic Missile Division HQ Air Research & Development Command P. O. Box 262 Inglewood, California Attn: WDTLAR	1
Chief, Defense Atomic Support Agency Washington 25, D. C. Attn: Document Library	1
Headquarters, Arnold Engineering Development Center Air Research and Development Center Arnold Air Force Station, Tennessee Attn: Technical Library Attn: AEOR Attn: AEOIM	1 1 1
Commanding Officer, DOFL Washington 25, D. C. Attn: Library, Room 211, Bldg. 92	1
Commanding General Redstone Arsenal Huntsville, Alabama Attn: Mr. N. Shapiro (ORDDW-MRF) Attn: Technical Library	1 1

AERODYNAMICS DEPARTMENT
EXTERNAL DISTRIBUTION LIST (A1)

	No. of Copies
NASA George C. Marshall Space Flight Center Huntsville, Alabama	
Attn: Dr. E. Geissler	1
Attn: Mr. T. Reed	1
Attn: Mr. H. Paul	1
Attn: Mr. W. Dahm	1
Attn: Mr. D. Burrows	1
Attn: Mr. J. Kingsbury	1
Attn: ORDAB-DA	1
APL/JHU (C/NOw 7386) 8621 Georgia Avenue Silver Spring, Maryland	
Attn: Technical Reports Group	2
Attn: Mr. D. Fox	1
Attn: Dr. F. Hill Via: INSORD	1
Air Force Systems Command Scientific & Technical Liaison Office Room 2305, Munitions Building Department of the Navy Washington 25, D. C.	
Attn: E. G. Haas	1

AERODYNAMICS DEPARTMENT
EXTERNAL DISTRIBUTION LIST (A2)

	No. of Copies
University of Minnesota Minneapolis 14, Minnesota	
Attn: Dr. E. R. G. Eckert	1
Attn: Heat Transfer Laboratory	1
Attn: Technical Library	1
Rensselaer Polytechnic Institute Troy, New York	
Attn: Dept. of Aeronautical Engineering	1
Dr. James P. Hartnett Department of Mechanical Engineering University of Delaware Newark, Delaware	1
Princeton University James Forrestal Research Center Gas Dynamics Laboratory Princeton, New Jersey	
Attn: Prof. S. Bogdonoff	1
Attn: Dept. of Aeronautical Engineering Library	1
Defense Research Laboratory The University of Texas P. O. Box 8029 Austin 12, Texas	
Attn: Assistant Director	1
Ohio State University Columbus 10, Ohio	
Attn: Security Officer	1
Attn: Aerodynamics Laboratory	1
Attn: Dr. J. Lee	1
Attn: Chairman, Dept. of Aero. Engineering	1
California Institute of Technology Pasadena, California	
Attn: Guggenheim Aero. Laboratory, Aeronautics Library	1
Attn: Jet Propulsion Laboratory	1
Attn: Dr. H. Liepmann	1
Attn: Dr. L. Lees	1
Attn: Dr. D. Coles	1
Attn: Mr. A. Roshko	1
Attn: Dr. J. Laufer	1
Case Institute of Technology Cleveland 6, Ohio	
Attn: G. Kuerti	1

AERODYNAMICS DEPARTMENT
EXTERNAL DISTRIBUTION LIST (A2)

	No. of Copies
North American Aviation, Inc. Aerophysics Laboratory Downing, California	
Attn: Dr. E. R. Van Driest	1
Attn: Missile Division (Library)	1
Department of Mechanical Engineering Yale University 400 Temple Street New Haven 10, Connecticut	
Attn: Dr. P. P. Wegener	1
Attn: Prof. N. A. Hall	1
MIT Lincoln Laboratory Lexington, Massachusetts	1
RAND Corporation 1700 Main Street Santa Monica, California	
Attn: Library, USAF Project RAND	1
Attn: Technical Communications	1
Mr. J. Lukasiewicz Chief, Gas Dynamics Facility ARO, Incorporated Tullahoma, Tennessee	1
Massachusetts Institute of Technology Cambridge 39, Massachusetts	
Attn: Prof. J. Kaye	1
Attn: Prof. M. Finston	1
Attn: Mr. J. Baron	1
Attn: Prof. A. H. Shapiro	1
Attn: Naval Supersonic Laboratory	1
Attn: Aero. Engineering Library	1
Polytechnic Institute of Brooklyn 527 Atlantic Avenue Freeport, New York	
Attn: Dr. A. Ferri	1
Attn: Dr. M. Bloom	1
Attn: Dr. P. Libby	1
Attn: Aerodynamics Laboratory	1
Brown University Division of Engineering Providence, Rhode Island	
Attn: Prof. R. Probstein	1
Attn: Prof. C. Lin	1
Attn: Librarian	1

AERODYNAMICS DEPARTMENT
EXTERNAL DISTRIBUTION LIST (A2)

	No. of Copies
Air Ballistics Laboratory Army Ballistic Missile Agency Huntsville, Alabama	1
Applied Mechanics Reviews Southwest Research Institute 8500 Culebra Road San Antonio 6, Texas	1
BuWeps Representative Aerojet-General Corporation 6352 N. Irwindale Avenue Azusa, California	1
Boeing Airplane Company Seattle, Washington	
Attn: J. H. Russell	1
Attn: Research Library	1
United Aircraft Corporation 400 Main Street East Hartford 8, Connecticut	
Attn: Chief Librarian	1
Attn: Mr. W. Kuhrt, Research Dept.	2
Attn: Mr. J. G. Lee	1
Hughes Aircraft Company Florence Avenue at Teale Streets Culver City, California	
Attn: Mr. D. J. Johnson R&D Technical Library	1
McDonnell Aircraft Corporation P. O. Box 516 St. Louis 3, Missouri	1
Lockheed Missiles and Space Company P. O. Box 504 Sunnyvale, California	
Attn: Dr. L. H. Wilson	1
Attn: Mr. M. Tucker	1
Attn: Mr. R. Smelt	1
The Martin Company Baltimore 3, Maryland	
Attn: Library	1
Attn: Chief Aerodynamicist	1

AERODYNAMICS DEPARTMENT
EXTERNAL DISTRIBUTION LIST (A2)

	No. of Copies
CONVAIR A Division of General Dynamics Corporation Fort Worth, Texas	
Attn: Library	1
Attn: Theoretical Aerodynamics Group	1
Purdue University School of Aeronautical & Engineering Sciences LaFayette, Indiana	
Attn: R. L. Taggart, Library	1
University of Maryland College Park, Maryland	
Attn: Director	2
Attn: Dr. J. Burgers	1
Attn: Librarian, Engr. & Physical Sciences	1
Attn: Librarian, Institute for Fluid Dynamics and Applied Mathematics	1
University of Michigan Ann Arbor, Michigan	
Attn: Dr. A. Kuethe	1
Attn: Dr. O. Laporte	1
Attn: Department of Aeronautical Engineering	1
Stanford University Palo Alto, California	
Attn: Applied Mathematics & Statistics Lab.	1
Attn: Prof. D. Bershader, Dept. of Aero. Engr.	1
Cornell University Graduate School of Aeronautical Engineering Ithaca, New York	
Attn: Prof. W. R. Sears	1
The Johns Hopkins University Charles and 34th Streets Baltimore, Maryland	
Attn: Dr. F. H. Clauser	1
Attn: Dr. M. Morkovin	1
University of California Berkeley 4, California	
Attn: G. Maslach	1
Attn: Dr. S. Schaaf	1
Attn: Dr. Holt	1
Attn: Institute of Engineering Research	1

AERODYNAMICS DEPARTMENT
EXTERNAL DISTRIBUTION LIST (A2)

	No. of Copies
Cornell Aeronautical Laboratory, Inc. 4455 Genesee Street Buffalo 21, New York	
Attn: Librarian	1
Attn: Dr. Franklin Moore	1
Attn: Dr. J. G. Hall	1
University of Minnesota Rosemount Research Laboratories Rosemount, Minnesota	
Attn: Technical Library	1
Director, Air University Library Maxwell Air Force Base, Alabama	1
Douglas Aircraft Company, Inc. Santa Monica Division 3000 Ocean Park Boulevard Santa Monica California	
Attn: Chief Missiles Engineer	1
Attn: Aerodynamics Section	1
General Motors Corporation Defense Systems Division Santa Barbara, California	
Attn: Dr. A. C. Charters	1
CONVAIR A Division of General Dynamics Corporation Daingerfield, Texas	1
CONVAIR Scientific Research Laboratory 5001 Kearney Villa Road San Diego 11, California	1
Attn: Asst. to the Director of Scientific Research	1
Attn: Dr. B. M. Leadon	1
Attn: Library	1
Republic Aviation Corporation Farmingdale, New York	
Attn: Technical Library	1
General Applied Science Laboratories, Inc. Merrick and Stewart Avenues Westbury, L. I., New York	
Attn: Mr. Walter Daskin	1
Attn: Mr. R. W. Byrne	1

AERODYNAMICS DEPARTMENT
EXTERNAL DISTRIBUTION LIST (A2)

	No. of Copies
Arnold Research Organization, Inc. Tullahoma, Tennessee	
Attn: Technical Library	1
Attn: Chief, Propulsion Wind Tunnel	1
Attn: Dr. J. L. Potter	1
General Electric Company Missile and Space Vehicle Department 3198 Chestnut Street Philadelphia, Pennsylvania	
Attn: Larry Chasen, Mgr. Library	2
Attn: Mr. R. Kirby	1
Attn: Dr. J. Farber	1
Attn: Dr. G. Sutton	1
Attn: Dr. J. D. Stewart	1
Attn: Dr. S. M. Scala	1
Attn: Dr. H. Lew	1
Attn: Mr. J. Persh	1
Eastman Kodak Company Navy Ordnance Division 50 West Main Street Rochester 14, New York	
Attn: W. B. Forman	2
Library AVCO-Everett Research Laboratory 2385 Revere Beach Parkway Everett 49, Massachusetts	3
AVCO-Everett Research Laboratory 201 Lowell Street Wilmington, Massachusetts	
Attn: Mr. F. R. Riddell	1
AER, Incorporated 158 North Hill Avenue Pasadena, California	1
Armour Research Foundation 10 West 35th Street Chicago 16, Illinois	
Attn: Dept. M	2
Attn: Dr. Paul T. Torda	1
Chance-Vought Aircraft, Inc. Dallas, Texas	
Attn: Librarian	2

AERODYNAMICS DEPARTMENT
EXTERNAL DISTRIBUTION LIST (A2)

	No. of Copies
National Science Foundation 1951 Constitution Avenue, N. W. Washington 25, D. C. Attn: Engineering Sciences Division	1
New York University University Heights New York 53, New York Attn: Department of Aeronautical Engineering	1
New York University 25 Waverly Place New York 3, New York Attn: Library, Institute of Math. Sciences	1
NORAIR A Division of Northrop Corp. Hawthorne, California Attn: Library	1
Northrop Aircraft, Inc. Hawthorne, California Attn: Library	1
Gas Dynamics Laboratory Technological Institute Northwestern University Evanston, Illinois Attn: Library	1
Pennsylvania State University University Park, Pennsylvania Attn: Library, Dept. of Aero. Engineering	1
The Ramo-Wooldridge Corporation 8820 Bellanca Avenue Los Angeles 45, California	1
Gifts and Exchanges Fondren Library Rice Institute P. O. Box 1892 Houston 1, Texas	1
University of Southern California Engineering Center Los Angeles 7, California Attn: Librarian	1

AERODYNAMICS DEPARTMENT
EXTERNAL DISTRIBUTION LIST (A2)

	No. of Copies
Commander Air Force Flight Test Center Edwards Air Force Base Muroc, California Attn: FTOTL	1
Air Force Office of Scientific Research Holloman Air Force Base Alamogordo, New Mexico Attn: SRLTL	1
The Editor Battelle Technical Review Battelle Memorial Institute 505 King Avenue Columbus 1, Ohio	1
Douglas Aircraft Company, Inc. El Segundo Division El Segundo, California	1
Fluidyne Engineering Corp. 5740 Wayzata Blvd. Golden Valley Minneapolis 16, Minnesota	1
Grumman Aircraft Engineering Corp. Bethpage, L. I., New York	1
Lockheed Missile and Space Company P. O. Box 551 Burbank, California Attn: Library	1
Marquardt Aircraft Corporation 7801 Havenhurst Van Nuys, California	1
The Martin Company Denver, Colorado Attn: Library	1
Mississippi State College Engineering and Industrial Research Station Aerophysics Department P. O. Box 248 State College, Mississippi	1

AERODYNAMICS DEPARTMENT
EXTERNAL DISTRIBUTION LIST (A2)

	No. of Copies
Lockheed Missile and Space Company 3251 Hanover Street Palo Alto, California	
Attn: Mr. J. A. Laurmann	1
Attn: Library	
General Electric Company Research Laboratory Schenectady, New York	
Attn: Dr. H. T. Nagamatsu	1
Attn: Library	
Fluid Dynamics Laboratory Mechanical Engineering Department Stevens Institute of Technology Hoboken, New Jersey	
Attn: Dr. R. H. Page, Director	1
Department of Mechanical Engineering University of Arizona Tucson, Arizona	
Attn: Dr. E. K. Parks	1
Vitro Laboratories 200 Pleasant Valley Way West Orange, New Jersey	
Attn: Dr. Charles Sheer	1
Department of Aeronautical Engineering University of Washington Seattle 5, Washington	
Attn: Prof. R. E. Street	1
Attn: Library	1
Aeronautical Engineering Review 2 East 64th Street New York 21, New York	1
Institute of the Aerospace Sciences 2 East 64th Street New York 21, New York	
Attn: Managing Editor	1
Attn: Library	1
Department of Aeronautics United States Air Force Academy Colorado	1

AERODYNAMICS DEPARTMENT
EXTERNAL DISTRIBUTION LIST (A2)

	No. of Copies
MHD Research, Inc. Newport Beach, California Attn: Dr. V. H. Blackman, Technical Director	1
University of Alabama College of Engineering University, Alabama Attn: Prof. C. H. Bryan, Head Dept. of Aeronautical Engineering	1
Office of Naval Research Bldg. T-3, Department of the Navy 17th and Constitution Avenue Washington 25, D. C. Attn: Mr. Ralph D. Cooper, Head Fluid Dynamics Branch	1
ARDE Associates 100 W. Century Road Paramus, New Jersey Attn: Mr. Edward Cooperman	1
Aeronautical Research Associates of Princeton 50 Washington Road Princeton, New Jersey Attn: Dr. C. duP. Donaldson, President	1
Daniel Guggenheim School of Aeronautics Georgia Institute of Technology Atlanta, Georgia Attn: Prof. A. L. Ducoffe	1
University of Cincinnati Cincinnati, Ohio Attn: Prof. R. P. Harrington, Head Dept. of Aeronautical Engineering Prof. Ting Yi Li	1 1
Virginia Polytechnic Institute Dept. of Aerospace Engineering Blacksburg, Virginia Attn: Mr. R. T. Keefe Attn: Library	1 1
IBM Federal System Division 7220 Wisconsin Avenue Bethesda, Maryland Attn: Dr. I. Korobkin	1

AERODYNAMICS DEPARTMENT
EXTERNAL DISTRIBUTION LIST (A2)

	No. of Copies
Superintendent U. S. Naval Postgraduate School Monterey, California Attn: Technical Reports Section Library	1
National Bureau of Standards Washington 25, D. C. Attn: Chief, Fluid Mechanics Section	1
North Carolina State College Raleigh, North Carolina Attn: Prof. R. W. Truitt, Head Dept. of Mechanical Engineering	1
Attn: Division of Engineering Research Technical Library	1
Apollo - DDCS General Electric Company A&E Bldg., Rm. 204 Daytona Beach, Florida Attn: Dave Hovis	1

CATALOGING INFORMATION FOR LIBRARY USE

BIBLIOGRAPHIC INFORMATION

	DESCRIPTORS	CODES		DESCRIPTORS	CODES
SOURCE	NOL technical report	NOLTR	SECURITY CLASSIFICATION AND CODE COUNT	Unclassified - 25	U025
REPORT NUMBER	63--77	63ØØ77	CIRCULATION LIMITATION		
REPORT DATE	3 July 1963	Ø763	CIRCULATION LIMITATION OR BIBLIOGRAPHIC		
			BIBLIOGRAPHIC (SUPPL., VOL., ETC.)		

SUBJECT ANALYSIS OF REPORT

DESCRIPTORS	CODES	DESCRIPTORS	CODES	DESCRIPTORS	CODES
Turbulent	TUBU	Relation	RELT	Fixed	FIXE
Boundary layer	BOUL	Shear	SHER		
Flat	FLAT	Sum	SUMS		
Plate	PLAT	Molecular	MOLC		
Friction	FRIC	Eddy	EDDI		
Heat transfer	HEAF	Viscosity	VISC		
Mass	MASZ	Gradient	GRDI		
Transfer	TRAE	Temperature	TEMP		
Coefficient	COEF	Concentration	CNCT		
Velocity	VELC	Aerodynamics	AERD		
Profile	PROF	Theory	THEY		
Calculation	COMA	Distribution	DISR		

PRNC-NOL-5070/28 (5-62)

Naval Ordnance Laboratory, White Oak, Md.
(NOL technical report 63-77)
A SEMI-EMPHIRICAL DERIVATION OF FRICTION, HEAT-TRANSFER, AND MASS-TRANSFER COEFFICIENTS FOR THE CONSTANT PROPERTY TURBULENT BOUNDARY LAYER ON A FLAT PLATE (U), by Neal Tetervin. 3 July 1963. 33p. charts, tables. Task NOL 364
UNCLASSIFIED

In this new method the friction coefficient and velocity profile are calculated from the relation between the shear, the sum of the molecular and eddy viscosity, and the velocity gradient. The entire velocity profile, from wall to outer edge, is calculable for all Reynolds numbers without using the concept of laminar sublayer, transition region, logarithmic region, etc. The heat and mass transfer coefficients and the temperature and concentration profiles are calculated by a similar method.
Abstract card is unclassified

1. Plates, Flat - Boundary layer
2. Boundary layer, Turbulent

I. Title
II. Tetervin, Neal
III. Project

Naval Ordnance Laboratory, White Oak, Md.
(NOL technical report 63-77)
A SEMI-EMPHIRICAL DERIVATION OF FRICTION, HEAT-TRANSFER, AND MASS-TRANSFER COEFFICIENTS FOR THE CONSTANT PROPERTY TURBULENT BOUNDARY LAYER ON A FLAT PLATE (U), by Neal Tetervin. 3 July 1963. 33p. charts, tables. Task NOL 364
UNCLASSIFIED

In this new method the friction coefficient and velocity profile are calculated from the relation between the shear, the sum of the molecular and eddy viscosity, and the velocity gradient. The entire velocity profile, from wall to outer edge, is calculable for all Reynolds numbers without using the concept of laminar sublayer, transition region, logarithmic region, etc. The heat and mass transfer coefficients and the temperature and concentration profiles are calculated by a similar method.
Abstract card is unclassified

1. Plates, Flat - Boundary layer
2. Boundary layer, Turbulent

I. Title
II. Tetervin, Neal
III. Project

Naval Ordnance Laboratory, White Oak, Md.
(NOL technical report 63-77)
A SEMI-EMPHIRICAL DERIVATION OF FRICTION, HEAT-TRANSFER, AND MASS-TRANSFER COEFFICIENTS FOR THE CONSTANT PROPERTY TURBULENT BOUNDARY LAYER ON A FLAT PLATE (U), by Neal Tetervin. 3 July 1963. 33p. charts, tables. Task NOL 364
UNCLASSIFIED

In this new method the friction coefficient and velocity profile are calculated from the relation between the shear, the sum of the molecular and eddy viscosity, and the velocity gradient. The entire velocity profile, from wall to outer edge, is calculable for all Reynolds numbers without using the concept of laminar sublayer, transition region, logarithmic region, etc. The heat and mass transfer coefficients and the temperature and concentration profiles are calculated by a similar method.
Abstract card is unclassified

1. Plates, Flat - Boundary layer
2. Boundary layer, Turbulent

I. Title
II. Tetervin, Neal
III. Project

Naval Ordnance Laboratory, White Oak, Md.
(NOL technical report 63-77)
A SEMI-EMPHIRICAL DERIVATION OF FRICTION, HEAT-TRANSFER, AND MASS-TRANSFER COEFFICIENTS FOR THE CONSTANT PROPERTY TURBULENT BOUNDARY LAYER ON A FLAT PLATE (U), by Neal Tetervin. 3 July 1963. 33p. charts, tables. Task NOL 364
UNCLASSIFIED

In this new method the friction coefficient and velocity profile are calculated from the relation between the shear, the sum of the molecular and eddy viscosity, and the velocity gradient. The entire velocity profile, from wall to outer edge, is calculable for all Reynolds numbers without using the concept of laminar sublayer, transition region, logarithmic region, etc. The heat and mass transfer coefficients and the temperature and concentration profiles are calculated by a similar method.
Abstract card is unclassified

1. Plates, Flat - Boundary layer
2. Boundary layer, Turbulent

I. Title
II. Tetervin, Neal
III. Project

Naval Ordnance Laboratory, White Oak, Md.
(NOL technical report 63-77)
A SEMI-EMPHIRICAL DERIVATION OF FRICTION, HEAT-TRANSFER, AND MASS-TRANSFER COEFFICIENTS FOR THE CONSTANT PROPERTY TURBULENT BOUNDARY LAYER ON A FLAT PLATE (U), by Neal Tetervin. 3 July 1963. 33p. charts, tables. Task NOL 364
UNCLASSIFIED

In this new method the friction coefficient and velocity profile are calculated from the relation between the shear, the sum of the molecular and eddy viscosity, and the velocity gradient. The entire velocity profile, from wall to outer edge, is calculable for all Reynolds numbers without using the concept of laminar sublayer, transition region, logarithmic region, etc. The heat and mass transfer coefficients and the temperature and concentration profiles are calculated by a similar method.
Abstract card is unclassified

1. Plates, Flat - Boundary layer
2. Boundary layer, Turbulent
I. Title
II. Tetervin, Neal
III. Project

Naval Ordnance Laboratory, White Oak, Md.
(NOL technical report 63-77)
A SEMI-EMPHIRICAL DERIVATION OF FRICTION, HEAT-TRANSFER, AND MASS-TRANSFER COEFFICIENTS FOR THE CONSTANT PROPERTY TURBULENT BOUNDARY LAYER ON A FLAT PLATE (U), by Neal Tetervin. 3 July 1963. 33p. charts, tables. Task NOL 364
UNCLASSIFIED

In this new method the friction coefficient and velocity profile are calculated from the relation between the shear, the sum of the molecular and eddy viscosity, and the velocity gradient. The entire velocity profile, from wall to outer edge, is calculable for all Reynolds numbers without using the concept of laminar sublayer, transition region, logarithmic region, etc. The heat and mass transfer coefficients and the temperature and concentration profiles are calculated by a similar method.
Abstract card is unclassified

1. Plates, Flat - Boundary layer
2. Boundary layer, Turbulent
I. Title
II. Tetervin, Neal
III. Project

Naval Ordnance Laboratory, White Oak, Md.
(NOL technical report 63-77)
A SEMI-EMPHIRICAL DERIVATION OF FRICTION, HEAT-TRANSFER, AND MASS-TRANSFER COEFFICIENTS FOR THE CONSTANT PROPERTY TURBULENT BOUNDARY LAYER ON A FLAT PLATE (U), by Neal Tetervin. 3 July 1963. 33p. charts, tables. Task NOL 364
UNCLASSIFIED

In this new method the friction coefficient and velocity profile are calculated from the relation between the shear, the sum of the molecular and eddy viscosity, and the velocity gradient. The entire velocity profile, from wall to outer edge, is calculable for all Reynolds numbers without using the concept of laminar sublayer, transition region, logarithmic region, etc. The heat and mass transfer coefficients and the temperature and concentration profiles are calculated by a similar method.
Abstract card is unclassified

1. Plates, Flat - Boundary layer
2. Boundary layer, Turbulent
I. Title
II. Tetervin, Neal
III. Project

Naval Ordnance Laboratory, White Oak, Md.
(NOL technical report 63-77)
A SEMI-EMPHIRICAL DERIVATION OF FRICTION, HEAT-TRANSFER, AND MASS-TRANSFER COEFFICIENTS FOR THE CONSTANT PROPERTY TURBULENT BOUNDARY LAYER ON A FLAT PLATE (U), by Neal Tetervin. 3 July 1963. 33p. charts, tables. Task NOL 364
UNCLASSIFIED

In this new method the friction coefficient and velocity profile are calculated from the relation between the shear, the sum of the molecular and eddy viscosity, and the velocity gradient. The entire velocity profile, from wall to outer edge, is calculable for all Reynolds numbers without using the concept of laminar sublayer, transition region, logarithmic region, etc. The heat and mass transfer coefficients and the temperature and concentration profiles are calculated by a similar method.
Abstract card is unclassified

1. Plates, Flat - Boundary layer
2. Boundary layer, Turbulent
I. Title
II. Tetervin, Neal
III. Project

UNCLASSIFIED